

Comprehensive Non-targeted Molecular Characterization of Organic Aerosols in the Amazon Rainforest

Denis Leppa^{*1}, ~~and~~ Stefanie Hildmann^{*1}, Nora Zannoni^{2,a}, Leslie A. Kremper^{2,c}, Bruna A. Holanda^{2,c}, Jonathan Williams^{2,3}, Christopher Pöhlker², Stefan Wolff^{2,b}, Marta Sà⁴, Maria Christina Solci⁵, Ulrich Pöschl², Thorsten Hoffmann¹

¹Chemistry Department, Johannes Gutenberg - University, Mainz, 55128, Germany

²[Multiphase Chemistry Department](#), Max Planck-Institute for Chemistry, Mainz, 55128, Germany

³Climate and Atmosphere Research Center, The Cyprus Institute, Nicosia, Cyprus

⁴Large-Scale Biosphere–Atmosphere Experiment in Amazonia (LBA), Instituto Nacional de Resquisas da Amazônia/INPA, Manaus, AM, Brazil

⁵Department of Chemistry Universidade Estadual de Londrina, Londrina, PR, Brazil

^anow at: Institute of Atmospheric Sciences and Climate, National Research Council (CNR-ISAC), 40129 Bologna, Italy

^bnow at: German Weather Service, Offenbach am Main, 63067, Germany

^cnow at: Hessian Agency for Nature Conservation, Environment and Geology, Wiesbaden, Germany

[*These authors contributed equally to this work.](#)

Correspondence to: Thorsten Hoffmann (t.hoffmann@uni-mainz.de)

Abstract

The Amazon rainforest plays a crucial role in the global climate system, hydrological cycle, and earth's energy balance. As one of the planet's least industrialized regions, it allows investigation of organic aerosol formation and constituents under almost pristine conditions. Nevertheless, human activities are known to affect this ecosystem – especially during the dry seasons. In this study, ambient aerosol samples collected at the Amazon Tall Tower Observatory (ATTO) during two dry and two wet seasons were characterized by high-resolution mass spectrometry (HR-MS). Comprehensive non-targeted data evaluation was applied to identify thousands of molecular formulae. Most were found to be associated with oxidation products of isoprene and monoterpenes, highlighting the predominance of biogenic secondary organic aerosols (SOA) at ATTO. The chemical composition exhibited distinct seasonal patterns with more processed organic compounds during the dry season, which can be explained by an increase of later-generation oxidation products due to reduced wet deposition and enhanced long-range transport. Mono- and polycyclic heteroaromatic components from biomass burning (BB) sources were enhanced during the dry seasons and the second wet season. The wet seasons were generally characterized by less oxidized compounds, associated with freshly formed SOA particles. Height-resolved measurements showed the forest canopy to be the main source for biogenic emissions with higher concentrations of early terpene oxidation products at lower altitudes lower down. Overall, our results provide new insights into the molecular characteristics and seasonality of organic particulate matter at ATTO, helping to constrain the sources and interactions of aerosols, clouds, and precipitation in the Amazon rainforest.

hat formatiert: Schriftfarbe: Text 1

hat formatiert: Schriftfarbe: Text 1

1 Introduction

Organic particulate matter (PM) accounts for up to 90 % of the total atmospheric aerosol mass (Kanakidou et al., 2005; Kroll and Seinfeld, 2008; Jimenez et al., 2009). While primary organic aerosols (POA) are emitted directly into the atmosphere (e.g., combustion of biomass), secondary organic aerosols (SOA) are produced by oxidative processes and transformations of volatile organic compounds (VOC), followed by their [oxidation products](#)' nucleation and/or condensation in the atmosphere (Seinfeld and Pankow, 2003). Numerous studies have illustrated the complex chemical composition of organic aerosols covering various compound classes and thousands of different organic species (Tolocka et al., 2004; Zhang et al., 2007; Goldstein and Galbally, 2007; Wozniak et al., 2008; Nizkorodov et al., 2011). Organic aerosols have a substantial impact on climate and human health (Pöschl, 2005; Hallquist et al., 2009). Consequently, clarifying the chemical composition of organic aerosols is an essential task of atmospheric-related studies.

Compounds in OA feature a huge variety of functionalities, polarities, and volatilities at various concentration regimes (Goldstein and Galbally, 2007) which poses major challenges for analytical techniques (Nozière et al., 2015). Traditional gas chromatography and liquid chromatography systems coupled with mass spectrometry (GC/MS, LC/MS) have proven useful in identifying certain OA species (Hoffmann et al., 2011). However, these methods are limited to compounds with specific physicochemical properties and, thus, not adequate to resolve complex organic mixtures (Hildmann and Hoffmann, 2024). Hence, high-resolution mass spectrometry (HR-MS) with enhanced resolving power ($\geq 100\ 000$) and high mass accuracy (≤ 5 ppm) has received more and more attention in atmospheric aerosol research (Nozière et al., 2015; Burgay et al., 2023; Xie and Laskin, 2024). The combination with soft ionization methods, such as electrospray ionization (ESI), allows a detailed characterization of complex OA samples (Nizkorodov et al., 2011). Several studies have already proven the potential of HR-MS in smog chamber experiments (Thoma et al., 2022; Frauenheim et al., 2024). Hundreds of different organic species have been detected in SOA samples generated by isoprene and monoterpene oxidation (Tolocka et al., 2004; Bateman et al., 2008; Nguyen et al., 2010). Additionally, OA samples from urban and pristine environments have been analyzed by HR-MS to identify transformation processes and potential sources of aerosol constituents (Wang et al., 2017; Tong et al., 2016; Kourtchev et al., 2013; Hettiyadura et al., 2021; Lin et al., 2018).

The Amazon basin is one of the most pristine ecosystems on Earth, comprising approximately 40% of all tropical forests (Goulding and Barthem, 2003; Baccini et al., 2012). The ecosystem impacts the earth's climate through its role in the hydrological cycle, its role as storage for atmospheric carbon, and the radiative effects of its associated cloud systems. However, the Amazon region is heavily impacted by anthropogenic activities such as deforestation (Andreae et al., 2015). Observations and [modeling/modelling](#) studies show that climate change and deforestation affect the carbon and hydrological cycles in Amazonia, changing to carbon neutrality and affecting precipitation downwind (Artaxo et al., 2022). Consequently, significant seasonal fluctuations in OA concentrations are observed, influencing the radiation balance and cloud processing (Pöhlker et al., 2023; Pöschl et al., 2010; Artaxo et al., 2013). Despite the Amazon's pivotal role in the Earth's atmosphere, our comprehension of the underlying atmospheric processes remains incomplete. For instance, the role of organic compounds in nucleation, cloud formation processes, or the aging and processing of aerosol components remains unresolved. An understanding of these processes is a fundamental prerequisite for assessing the future of the ecosystem in the context of climate and land use change (Shrivastava et al., 2019). To address such questions, a molecular characterization of organic aerosol in the Amazon rainforest is required.

[In this study, LC-HR-MS was applied to analyze aerosol filter samples collected at the ATTO site during multiple campaigns across 2018 and 2019. Organic aerosols were sampled at distinct heights \(0 m, 42 m, 80 m, 150 m, and 320 m\) to investigate vertical gradients in chemical composition. This height-resolved sampling strategy was designed to capture the influence of biogenic emissions near the forest canopy, photochemical transformation processes above the canopy, and the impact of regionally transported, aged aerosol in the upper boundary layer. In particular, sub-canopy and near-canopy samples reflect](#)

85 local sources and early secondary organic aerosol formation, whereas the 320 m platform provides insight into regional and
long-range transport contributions. These data enable a more detailed separation of local and regional influences on OA
composition. It is important to note, however, that vertical differences are strongly influenced by seasonal and diurnal
meteorological variability, including boundary layer dynamics, atmospheric mixing, and air mass history. Thus, height-
90 resolution analytical techniques were employed to characterize the molecular composition of OA in relation to emission
sources, (trans)formation processes, and atmospheric conditions. This molecular-level understanding contributes to improved
representation of aerosol–cloud–climate interactions in atmospheric chemistry and climate models, particularly for pristine
yet rapidly changing tropical regions such as the Amazon.

In this study, LC-HR-MS was used to analyze aerosol filter samples from the Amazon rainforest covering several seasons
95 from 2018 and 2019. Sophisticated non-targeted analytical techniques were applied to link the OA molecular composition
with meteorological conditions, potential emission sources, and (trans)formation processes. The work provides a
comprehensive molecular-level understanding of organic aerosols in the Amazon rainforest, a key region for studying
interactions between natural and anthropogenic influences on the atmosphere. The Amazon's organic aerosols play a critical
role in regional and global climate regulation, biogeochemical cycles, and cloud formation processes. Despite their
100 significance, the molecular complexity and variability of these aerosols remain underexplored. By employing advanced non-
targeted analytical approaches, this study aims to fill knowledge gaps regarding their sources, transformations, and impacts,
ultimately contributing to improved models of atmospheric chemistry and climate dynamics.

2 Experimental section

2.1 Aerosol sampling

105 Ambient PM_{2.5} aerosol samples were collected in the Amazon rainforest at the Amazon Tall Tower Observatory (ATTO). In
total, four measurement campaigns were performed to investigate seasonal variations of the SOA chemical composition. The
sampling time covered the wet season 2018 (14/Apr/2018 – 19/Apr/2018), the dry season 2018 (22/Oct/2018 – 31/Oct/2018),
the wet season 2019 (04/Mar/2019 – 14/Mar/2019), and the dry season 2019 (20/Sep/2019 – 26/Sep/2019). The research site
allows height-resolved measurements on a 325 m tall tower in the central Amazon basin (coordinates: S 02°08.752' W
110 59°00.335') and is described in detail by Andreae et al. (2015). Shortly, the nearest urban region is Manaus which is located
approximately 150 km southwest of ATTO. The station is part of the Uatumã Sustainable Development Reserve (UDSR) and
is reached via the roughly 12 km distant Uatumã river. The tower is located at about 120 m above sea level on a plateau that
is embedded in a dense, non-flooded forest (terra firme) with adjacent floodplain forests and white-sand soil savannas
(campinas) and forests (campinaranas). The area at ATTO is characterized by a canopy height of about 35 m. The
115 meteorological conditions at ATTO depend on the location of the Intertropical Convergence Zone (ITCZ) providing clean and
rainy circumstances from February until May and polluted and drier conditions from August to November with strong
contributions from anthropogenic deforestation and land-use change (Pöhlker et al., 2019). Relevant meteorological
parameters were constantly measured and are shown in the supporting information. The corresponding wind profiles and
backward trajectories were generated by the HYSPLIT Trajectory Model (Stein et al., 2015; Rolph et al., 2017).

120 Ambient PM_{2.5} filter samples were collected at three different heights at the tower (wet season 2018: 42 m – 15 filters + 2
blank filters, 150 m – 14 filters + 2 blank filters, 320 m – 15 filters + 2 blank filters; dry season 2018 and wet season 2019:
80 m – 18 filters + 2 blank filters, 150 m – 18 filters + 2 blank filters, 320 m – 18 filters + 2 blank filters; wet season 2019: 80
m – 22 filters + 2 blank filters, 150 m – 22 filters + 2 blank filters, 320 m – 22 filters + 2 blank filters; dry season 2019: 0 m
– 16 filters + 2 blank filters, 80 m – 14 filters + 2 blank filters, 320 m – 16 filters + 2 blank filters,) using borosilicate glass
125 microfiber filter bonded with PTFE (Pallflex® Emfab, 70 mm diameter). A pre-separator (Digitel, DPM2.3) was set up in
front of the filter to only collect the size fraction with aerodynamic particle diameters below 2.5 µm at constant flow rates of

38 L min⁻¹. The sampling duration was set to 10 h – 14 h to allow daytime and nighttime related sample collection while ensuring sufficient particle mass on the filter material. Blank filters were collected according to the mentioned procedures but with disabled pumps. In total, 204246 filter samples were collected and stored in the freezer at -18 °C before their analysis.

2.2 Sample preparation and analysis

One half of each filter sample was extracted three times by adding 1.5 mL of a 9:1 mixture of methanol and water (Fisher Scientific, Optima™ grade). The samples were subsequently agitated for 30 min on a laboratory shaker. The combined liquid phases were filtered afterward through a 0.2 μm PTFE syringe filter (Carl Roth, Rotilabo® KC 94.1) and evaporated completely by a gentle stream of N₂. The residue was then reconstituted in 700 μL of a 9:1 mixture of water and acetonitrile (Fisher Scientific, Optima™ grade).

Ten microliters of each sample were analyzed three times by ultra high-performance liquid chromatography (UHPLC) (ThermoFisher Scientific, UltiMate 3000) coupled to a high-resolution Orbitrap mass spectrometer (MS) (ThermoFisher Scientific, Q Exactive™). A heated electrospray ionization (ESI) source was installed and operated in the negative ionization mode. The instrument was externally calibrated with a calibration solution (Fisher Scientific, Pierce™) and a 2 mM sodium acetate aqueous solution providing mass accuracies below 1 ppm. The sample analysis was performed in the range of *m/z* 50 – 750 at a mass resolving power of 140 000 at *m/z* 200. The following ESI-MS parameters were used for the measurements: ESI capillary temperature 300 °C; spray voltage -3.2 kV; sheath gas flow 30; auxiliary gas flow 10, S-lens RF level 50%. The UHPLC system was operated with a HSS T3 column (100 × 2.1 mm ID, 1.8 μm, Waters, ACQUITY UPLC®) and the mobile phase A (water with 2% acetonitrile and 0.04% formic acid) and mobile phase B (acetonitrile with 2% water). The conditions for gradient elution were as follows: 0 – 2 min 0% B, 2 – 9 min linear increase to 30% B, 9 – 15 min linear increase to 95% B, 15 – 17.5 min 95% B, 17.5 – 19 min linear decrease to 0% B, 19 – 21 min 0% B at a constant flow rate of 350 μL min⁻¹.

2.3 Non-Targeted Data Evaluation

The LC/MS data were processed by MzMine 2.30 to obtain molecular formulae C_cH_hO_oN_nS_s with the following limitations: 2 ≤ C ≤ 40, 2 ≤ H ≤ 100, 0 ≤ O ≤ 40, 0 ≤ N ≤ 4, 0 ≤ S ≤ 2. Fluorine was not taken into account in the data evaluation, although recent studies show that fluorine compounds in the form of per- and polyfluoroalkyl substances (PFAS) can also be detected in traces in aerosols over tropical rainforests (Kourtchev et al., 2024). The mass tolerance for the formula assignment was set to ± 2 ppm considering isotope patterns. Adducts were removed and only ions present in all three repeated measurements were retained. The signal intensities per sample were averaged afterward. Blank samples were processed accordingly and subtracted. Only compounds with signal-to-background ratios ≥ 3 were kept for further evaluations.

The number of rings and double bonds was described by the double bond equivalent (DBE) for each assigned formula providing information on the degree of unsaturation and calculated by equation (2.1) (Badertscher et al., 2001):

$$DBE = nc - \frac{n_H}{2} + \frac{n_N}{2} + \frac{n_S}{2} + 1 \quad (2.1)$$

where *n* describes the number of the respective element.

Based on the DBE values the aromaticity equivalent (Xc) was calculated by equation (2.2) to identify mono- and polycyclic aromatic compounds (Yassine et al. (2014)):

$$X_c = \frac{3(DBE - (p \cdot n_o + q \cdot n_s)) - 2}{DBE - (p \cdot n_o + q \cdot n_s)} \quad (2.2)$$

where p and q represent the fraction of oxygen and sulfur atoms that are involved in the π -bond structure of the molecule. Consequently, these values can vary according to different compound classes. While $p = q = 0.5$ is suggested for carboxylic acids, esters, and nitro functional groups, p and q are set to either 0 or 1 for aldehydes, ketones, alcohols, ethers, and nitroso classes. In the present study, $p = q = 0.5$ was used to calculate X_c considering that negative ESI analysis is highly sensitive to carboxylic acids (Kourtchev et al., 2016; Wang et al., 2017). According to Yassine et al. (2014), $X_c \geq 2.50$ and $X_c \geq 2.71$ are indicating monocyclic and polycyclic aromatic compounds, respectively.

The carbon oxidation state (OSC) for CHO compounds was calculated following the simplified equation (2.3) (Kroll et al. (2011)):

$$OSC \approx 2 \cdot \frac{n_o}{n_c} - \frac{n_H}{n_c} \quad (2.3)$$

with the elemental ratios O/C and H/C , respectively.

Furthermore, the saturation vapor pressure (C^0) has been calculated to predict the volatility of OA compounds according to equation (2.4) Donahue et al. (2011) and Li et al. (2016):

$$\log_{10} C^0 = (n_c^0 - n_c) \cdot b_c - n_o b_o - 2 \cdot \frac{n_c n_o}{n_c + n_o} \cdot b_{CO} - n_N b_N - n_S b_S \quad (2.4)$$

where n_c^0 describes the reference carbon number, b represents the contribution of each element to $\log_{10} C^0$, and b_{CO} denotes the carbon-oxygen nonideality. The C^0 values have been calculated for compound classes containing C, H, O, N, and S atoms. The parameters for the calculation based on Li et al. (2016) are listed in the supporting information Table S 1.

Kendrick mass (KM) analysis was used to assign homologous series of the detected compounds, which vary only in the number of a defined base unit (Kendrick, 1963; Hughey et al., 2001). In the present study, CH_2 was chosen as the base unit by rescaling the exact mass of 14.01565 to 14.00000. KM_{CH_2} was calculated according to equation (2.5) for each compound by renormalizing the exact mass scale (Hughey et al., 2001):

$$KM_{CH_2} = \text{exact mass} \cdot \left(\frac{14.00000}{14.01565} \right) \quad (2.5)$$

Subsequently, the Kendrick mass defect (KMD) was calculated by equation (2.6):

$$KMD_{CH_2} = \text{nominal KM} - KM_{CH_2} \quad (2.6)$$

where *nominal KM* describes the KM rounded to the next integer. Consequently, compounds differing only in their number of CH_2 units have the same KMD values. Homologous series can be identified as horizontal lines in KMD plots.

200 3 Results and Discussion

The chemical complexity of the OA samples is highly influenced by stochastic regional events and the respective meteorological conditions between sampling days, such as the height of the mixing layer and the wind direction. In order to take these influences into account, a distinction is made in the present study between background, variable and total organic aerosol compounds. Only compounds that were observed in more than 75 % of all samples based on their presence (identical molecular formula + retention time) were defined as background compounds. They presumably describe the local OA characteristics, as it is assumed that they are not dependent on individual emission events. For the variable OA characteristics, the evaluation was carried out by subtracting the peak areas of the previously determined background compounds from the peak areas of the –total number of identified compounds (= background compounds + variable compounds). The variable remaining compounds are attributed to irregular atmospheric events, presumably caused by different meteorological conditions. Compounds that were only detected once in the respective data set were excluded as they were not considered representative.

3.1 Total OA characteristics

All detected compounds were separated by reversed-phase HPLC prior to MS analysis, which increases the number of measurable compounds and reduces the risk of ion suppression in the ESI source. The chemical composition of the SOA samples was mainly influenced by seasonal effects during the measurement campaigns. A total of 2336 molecular formulas could be assigned, of which 699 were in the range of < 250 Da, 1309 between 250 Da and 450 Da, and 328 above > 450 Da. Typical mass spectra are shown in Figure S 20. Molecular weights (MW) in the range below 250 Da could be assigned to the majority of observed substances in both seasons, while the aerosol composition in the dry season additionally showed signals in the oligomeric range between 300 and 450 Da with lower intensity. While several studies have shown that ozonolysis of biogenic VOCs (e.g. α -pinene, β -pinene, isoprene) in smog chamber experiments produces compounds with high molecular weight and increased signal intensities in the oligomeric range (Kourtchev et al., 2014a; Reinhardt et al., 2007), molecules with MWs above 450 Da contributed insignificantly to the total number of compounds in the present filter samples.

All filter samples reveal a high chemical diversity with 875 – 1940 unambiguously assigned molecular formulae with a large fraction of isomeric compounds (69% – 85%) (Table I), highlighting the importance of pre-separating the samples by HPLC. The identified molecular formulae were divided into four subgroups according to their elemental composition: CHO, CHON, CHONS, and CHOS. The CHO subgroup is predominant with (56 \pm 6) % in all samples, followed by CHON with (20 \pm 7) %, CHOS (17 \pm 5) %, and CHONS (7 \pm 1) %, although the contribution of sulfur- and/or nitrogen-containing compounds increases at higher MWs. This trend is in good agreement with similar studies from remote environments (e.g. Amazonia, Brazil: CHO⁽⁻⁾ with 58-63 %, CHON⁽⁻⁾ with 25-30 %, CHOS⁽⁻⁾ with 10 %, CHONS⁽⁻⁾ with 2 %, Brazil, Kourtchev et al., 2016; Hyytiälä, Finland: CHO⁽⁻⁾ with 54.8 \pm 2.2 %, CHON⁽⁻⁾ with 21 \pm 3 %, CHOS⁽⁻⁾ with 16 \pm 3 %, CHONS⁽⁻⁾ with 5.4 \pm 2.2 %, Kourtchev et al., 2013), while studies from a suburban and urban environment revealed enhanced contributions of CHON and CHONS compounds (Pearl River Delta region, China: CHON⁽⁻⁾ with 34 %, CHONS⁽⁻⁾ with 8 %, Lin et al., 2012; Cambridge, UK: CHON⁽⁻⁾ with 33 %, CHONS⁽⁻⁾ with 21-26 %, Rincón et al., 2012; Shanghai, China: CHON⁽⁻⁾ with 21-23.7 %, CHONS⁽⁻⁾ with 11.2-16.6 %, Wang et al., 2017), proving an increased relevance of nitrogen and sulfur chemistry in more polluted areas.

The total calculated elemental ratios are highly variable throughout the seasonal measurement campaigns with 0.60 \pm 0.37 (mean value \pm standard deviation of the data set) and 1.47 \pm 0.49 for O/C and H/C during the dry season and 0.49 \pm 0.32 and 1.56 \pm 0.45 during the wet season, respectively. The wide variability indicates a high chemical complexity within the data set. Comparable values were reported from the boreal forest in Hyytiälä, Finland (0.58 and 1.54 for O/C and H/C, respectively) (Kourtchev et al., 2013). Additionally, the elemental ratios obtained in this study are consistent with smog chamber experiments using certain biogenic VOCs for SOA generation, e.g. α -pinene (0.42 – 0.55 for O/C and 1.5 for H/C, Putman et

hat formatiert: Schriftfarbe: Text 1

hat formatiert: Nicht Hervorheben

hat formatiert: Hochgestellt, Nicht Hervorheben

hat formatiert: Nicht Hervorheben

al., 2012) and limonene (0.5 – 0.6 for O/C and 1.5 – 1.6 for H/C, Kundu et al., 2012). Vertical profiles of α -pinene and limonene were measured at ATTO showing different chemical speciations between day and night (Zannoni et al., 2020; Yáñez-Serrano, 2018). The averaged total oxidation states of CHO compounds in the wet seasons ($-0.681 \leq \text{OSC} \leq -0.486$) are lower than in the dry seasons ($-0.525 \leq \text{OSC} \leq -0.324$) indicating more processed organic aerosol in the dry seasons than in the wet seasons. Furthermore, the averaged total aromaticity indices ($X_c \leq 2.50$) do not suggest a significant portion of mono- or polycyclic hydrocarbons.

Table I: Summary of all observed MS signals with unambiguous molecular formula assignment for the four measurement campaigns in 2018 and 2019 (wet season = WS, dry season = DS). The signals are divided into four subgroups regarding their elemental composition. The relative contribution of the subgroups was calculated by dividing the number of compounds of the particular subgroup by the total number of compounds. Additionally, the average values¹ of molecular weight (MW), carbon oxidation state (OSC), aromaticity index (Xc), and isomeric fraction are listed.

Season	Height m	Number of compounds detected	CHO %	CHON %	CHONS %	CHOS %	MW Da	OSC ²	Xc	Isomers %
WS18	42	1095	54	30	6	10	271	-0.647	0.872	77
	150	875	67	15	7	11	261	-0.606	0.977	80
	320	1293	43	41	7	9	293	-0.681	0.822	70
DS18	80	1856	51	19	7	23	245	-0.324	1.050	83
	150	1940	51	18	8	23	240	-0.353	1.051	85
	320	1720	52	18	8	22	245	-0.330	1.070	84
WS19	80	1555	55	19	5	21	250	-0.535	0.907	81
	150	1081	57	18	7	18	252	-0.486	0.922	81
	320	1287	62	17	6	15	255	-0.558	1.017	82
DS19	0	1328	60	17	5	18	237	-0.425	0.831	69
	80	1225	61	14	6	19	233	-0.439	0.906	84
	320	1050	62	15	6	17	246	-0.525	0.975	77

¹–Average values are calculated based on the molecular composition of each compound.

²–Only CHO compounds are considered in the calculation of OSC.

3.2 Background OA characteristics

A clear seasonality characterizes the molecular background composition of organic aerosols at ATTO. Air masses at ATTO are in response to the annual north-south migration of the ITCZ (Intertropical Convergence Zone) leading to a seasonal alternation between north-easterly winds during the wet seasons and south-easterly winds during the dry seasons (Pöhlker et al. 2019). Seven-day HYSPLIT backward trajectories (Stein et al., 2015) show that air masses need approximately 6 – 7 days from the west coast of Africa to pass the Atlantic Ocean towards ATTO (see-Figure S-42, Figure S-53). Higher wind speeds

of up to 15 – 20 m s⁻¹ were observed during the wet seasons (dry seasons 10-15 m s⁻¹), leading to a dilution of the particles phase at ATTO (Figure S-31). Comparable to cleaner marine air masses from the ocean, lower background signals are detected during the wet seasons. In contrast, the dry seasons are considerably influenced by biomass burning (Table S-3) and other anthropogenic emissions from the eastern regions in Brazil (Artaxo, 2002; Andreae et al., 2015), resulting in higher concentrations of particulate matter (PM) (Figure S-64, Figure S-75). Concentrations up to 15 µg m⁻³ have been observed during the dry periods while approximately ten times lower concentrations were detected during the wet season.

The chemical composition of background OA also reflects these seasonal changes in meteorological conditions. 72 – 215 organic compounds were detected during the dry seasons, while 28-60 different compounds were observed during the wet seasons (Table S-2). The molecular formulae in the wet seasons are predominated by the CHO subgroup (90 ± 7) %, followed by CHOS with (8 ± 7) %, CHONS (1 ± 1) %, and CHON (1 ± 2) %. The dry seasons show a comparable predominance of the CHO subgroup (93 ± 3) % and an equal contribution of CHONS compounds (1 ± 1) % but an increased fraction of CHON compounds (4 ± 1) % and a decreased fraction of CHOS compounds (3 ± 2) %. Furthermore, the averaged background aromaticity indices ($X_c \leq 2.50$) do not suggest a significant portion of mono- or polycyclic hydrocarbons in both seasons.

3.2.1 Van-Krevelen diagrams

Van Krevelen diagrams (VK diagrams) are used to visualize similarities and differences, e.g. between measuring locations, measuring heights, daily or seasonal influences. In a VK diagram, the H/C ratio is shown as a function of the O/C ratio for each molecular formula detected in a sample. This helps for example to visualize the degree of oxidation of the particle phase organics as the most oxidized molecules are located at the lower right corner (Zhang et al., 2021). Consequently, the most saturated and reduced species are found in the upper left region. VK diagrams of the wet and dry season 2018 at different sampling heights are shown in Figure 1. The corresponding VK diagrams for the wet and dry season 2019 show very similar patterns and can be found in Figure S-97. The signal intensity is proportional to the size of the symbols. However, the signal intensities of the various compounds certainly only provide semi-quantitative results and should therefore only be converted into concentrations to a limited extent, as different substances are detected with different sensitivities due to the selectivity of the electrospray ionization with regard to ion yield. The most intense ion signals are summarized in Table II with their molecular formula, their possible identity and the precursor species.

General: The background compounds in the wet seasons are all non-aromatics with a high O/C-ratio ($O/C \geq 0.5$) and either C4-5 or C7-8 backbones, probably resulting from isoprene and monoterpene (mainly α -pinene, β -pinene, and limonene) oxidation (Kleindienst et al., 2007; Nguyen et al., 2010; Worton et al., 2013; Hammes et al., 2019). These precursor compounds are the most prevalent biogenic VOCs in the Amazon rainforest, released by a large diversity of terrestrial vegetation (Guenther et al., 1995; Greenberg et al., 2004; Zannoni et al., 2020). The more complex chemical background of the dry seasons is clearly illustrated in the VK diagram in Figure 1. Especially the dry season 2018 was characterized by a high abundance of signals with H/C ratios ≥ 1.5 and O/C ratios ≤ 0.5 . These compounds are commonly attributed to aliphatic species, which can be related to both, biogenic and anthropogenic sources. Simultaneously, several compounds with low elemental ratios ($H/C \leq 1.0$ and $O/C \leq 0.5$) were identified as background compounds, typically associated with aromatic hydrocarbons (Wozniak et al., 2008; Mazzoleni et al., 2012). Species within this region were exclusively observed during the dry season 2018, where the highest particle concentrations were detected.

Isoprene SOA: The ion at m/z 149.0455 ($C_5H_{10}O_5$) was observed in all analyzed filter samples with high intensities. This component has been detected in isoprene oxidation chamber experiments and field studies using SOA filter sampling (Krechmer et al., 2015; Chen et al., 2020). $C_5H_{10}O_5$ was identified to be the most dominant species produced during the photooxidation of isoprene hydroxy hydroperoxides (ISOPOOH), which are important products of the isoprene oxidation under low-NO conditions (Krechmer et al., 2015; Paulot et al., 2009; Nagori et al., 2019). As shown in Figure S8, NO and

hat formatiert: Schriftart: Nicht Fett

hat formatiert: Schriftart: Nicht Fett

NO₂ mixing ratios were generally <0.5 ppb and <1 ppb at 73.3 m and <2 ppb and <0.5 ppb at 0.05 m for the dry season 2018.

hat formatiert: Tiefgestellt

For the wet seasons 2018 and 2019 NO mixing ratios were <0.25 ppb at 79.3 m and <1.5 ppb at 0.05 m whereas NO₂ mixing

hat formatiert: Tiefgestellt

ratios were <0.05 ppb at 79.3 m and <0.1 ppb at 0.05 m. NO_x data for the dry season 2019 are lacking due to instrument issues. These conditions are consistent with what is commonly defined as low-NO regimes in previous chamber studies (e.g.,

Krechmer et al., 2015; Paulot et al., 2009; Nagori et al., 2019). OH- initiated oxidation of ISOPOOH leads to only 2.5% to

hat formatiert: Tiefgestellt

organic aerosols including C₆H₁₀O₅, while approximately 90% result in the formation of isoprene epoxydiol (IEPOX) and

hat formatiert: Tiefgestellt

other gas-phase products (Krechmer et al., 2015). However, C₃H₁₀O₅ was also observed during isoprene ozonolysis and during

hat formatiert: Tiefgestellt

isoprene photooxidation under high-NO conditions (Jaoui et al., 2019). Consequently, the latter pathways appear to be the

dominant reactions during the dry seasons with increased NO concentrations (Figure S-68), while the ISOPOOH-SOA

pathway under low-NO conditions is presumed during the wet seasons.

IEPOX-OS: The samples from the 2018 wet season showed the ion at *m/z* 215.0231 (C₅H₁₂O₇S) as the most intense signal

hat formatiert: Schriftart: Nicht Fett

related to IEPOX-derived organosulfates (OS) (Surratt et al., 2007; Surratt et al., 2008). It is established that these OSs are

formed from the reactive uptake of IEPOX on acidic sulfate particles under low-NO conditions, which is in agreement with

our findings. IEPOX-OS was also found on filter samples from the Amazon rainforest in another study (Kourtchev et al.,

2016). The authors observed the highest intensities on filters highly affected by surrounding forest fires. Interestingly, the

lowest number of active fires was recorded during the wet season 2018 campaign (Table S 3) (INPE - Instituto Nacional de

Pesquisas Espaciais, 2020). Sulfate concentrations during the wet seasons are mainly attributed to biogenic and marine sources

(Andreae et al., 2015), while increased levels during drier seasons are related to combustion activities (Pöhlker et al., 2018).

Sulfur compounds can also be emitted from soils showing higher emissions with higher soil moisture (Pugliese et al., 2023)

leading to a significant organosulfur source from the forest itself. This suggests that IEPOX-OS is a relevant SOA constituent,

regardless of the current season, and is consistent with the idea of mixed anthropogenic and biogenic sources.

Monoterpene SOA: The wet season 2019 campaigns were characterized by intense ion signals at *m/z* 157.0506 (C₇H₁₀O₄)

hat formatiert: Schriftart: Nicht Fett

and *m/z* 171.0662 (C₈H₁₂O₄) (Fig S9), attributed to limonene and α -pinene oxidation products, among others (Hammes et al.,

hat formatiert: Nicht Hervorheben

2019; Eddingsaas et al., 2012; Thoma et al., 2022; Florou et al., 2024), suggesting that biogenic sources are dominant

hat formatiert: Nicht Hervorheben

the main contributors to SOA loading at ATTO. Furthermore, the intensities of α -pinene oxidation products were higher in the

hat formatiert: Nicht Hervorheben

dry than in the wet seasons. This can be explained by increased ambient temperatures (Fig S1; Fig S2) and photosynthetic

hat formatiert: Nicht Hervorheben

active radiation facilitating the emission rates of monoterpenes (Guenther et al., 1991; Kesselmeier and Staudt, 1999). This

hat formatiert: Nicht Hervorheben

also affects the diel variation with prevalent concentrations during the day.

hat formatiert: Englisch (Vereinigtes Königreich)

Aromatics: All detected ions were classified by their aromaticity equivalent Xc according to Yassine et al. (2014), in order

hat formatiert: Schriftart: Nicht Fett

to identify mono- and polycyclic aromatic species. While monocyclic structures such as benzene and functionalized

derivatives are indicated by values of Xc \geq 2.50, condensed polycyclic aromatic compounds are described by Xc \geq 2.71.

Naphthalene is the smallest polycyclic structure meeting this criterion (Yassine et al., 2014; Wang et al., 2017). The dry season

campaigns were accompanied by an increased number of active fires and biomass burning (Table S 3). Consequently, the

detected aromatic hydrocarbons are mainly attributed to anthropogenic sources (Henze et al., 2008).

Hydrocarbons: The dry season 2018 was characterized by the occurrence of several aromatic species with Xc values \geq 2.50

hat formatiert: Schriftart: Nicht Fett

(Figure S-8). The most intense signals correspond to the ions at *m/z* 149.0243 (C₈H₆O₃), *m/z* 164.0353 (C₈H₇NO₃), *m/z*

193.0505 (C₁₀H₁₀O₄), and *m/z* 207.0298 (C₁₀H₈O₃), each with DBE values \geq 6. These compounds were already identified as

relevant components of biomass burning activities. C₈H₆O₃ and C₁₀H₈O₃ were observed during naphthalene photooxidation

experiments in a chamber study (Kautzman et al., 2010; Chhabra et al., 2015; Thoma et al., 2022). Naphthalene and other

polycyclic aromatic hydrocarbons (PAH) have been related to wood combustion processes in the literature and are considered

to impact human health (Schauer et al., 2001; Chan et al., 2009; Samburova et al., 2016; Baumann et al., 2023). C₁₀H₁₀O₄

might be a product formed during the degradation of cellulose and lignin, two important biopolymers (Kong et al., 2021). The

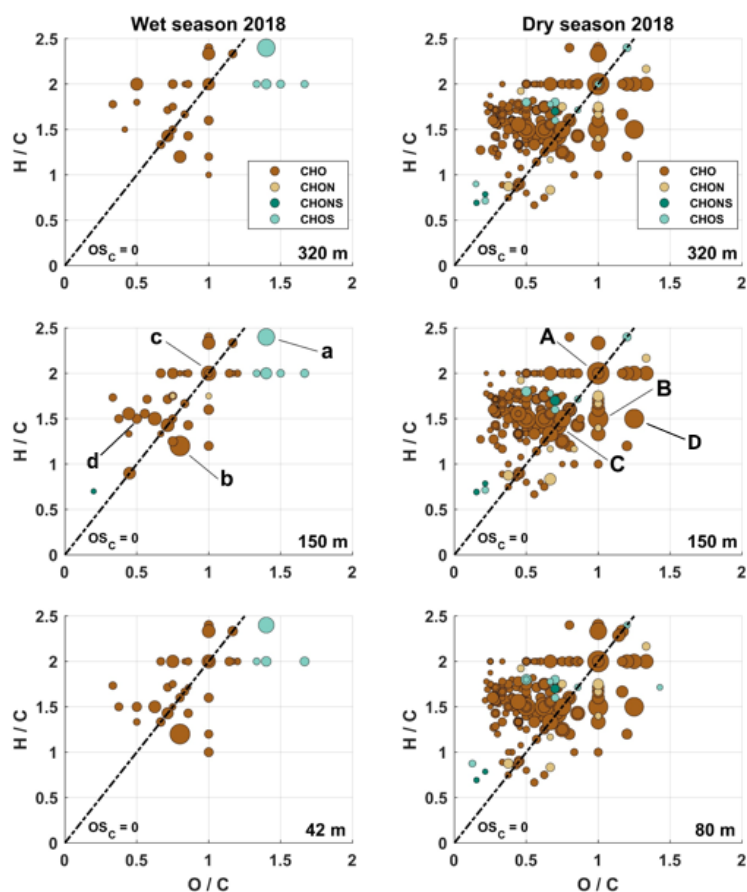
345 MS² spectrum (Figure S11-9) revealed two fragments, CO₂ and C₃H₄O₂ (acrylic acid), leading to a tentative structure of ferulic acid.

350 Nitro-hydrocarbons: C₈H₇NO₃ was assigned to a nitro-phenolic structure, which can be formed during biomass pyrolysis. This compound class is a major contributor to brown carbon (BrC) (Lin et al., 2016) and has been detected earlier in SOA samples from the Amazon rainforest (Claeys et al., 2012). The ion appeared in almost every sample of the dry season 2019 in high intensities, suggesting this compound to be an important biomass burning marker in this study. Another intense background ion was 4-nitrocatechol at *m/z* 154.0146 (C₆H₅NO₄), which has been previously considered as a marker compound for biomass burning OA (Iinuma et al., 2010; Claeys et al., 2012; Kourtchev et al., 2016).

355 Polycycles: The ion at *m/z* 219.0455 (C₁₅H₈O₂) appeared in the dry season 2019 samples and has already been reported in another study (Bruns et al., 2015). The authors identified this compound as an oxygenated PAH produced during wood combustion with a pyrene core structure, which seems reasonable according to the increased X_c Value of 2.82 and 12 DBE.

hat formatiert: Schriftart: Nicht Fett

hat formatiert: Schriftart: Nicht Fett



360 Figure 1: Van Krevelen plots from the wet season 2018 (left panel; sampling heights: 320 m, 150 m, 42 m) and the dry season 2018 (right panel; sampling heights: 320 m, 150 m, 80 m). Included are only molecular formulae that were present in more than 75% of the samples, respectively. The size of the data points represents the signal intensity of the corresponding peak. The four subgroups are distinguished with different colors. Compounds located on the black dashed line have an average carbon oxidation state of 0 (OS_c = 0). The labels a-d and A-D correspond to the most intense signals further characterized in Table II.

Table II: Possible identities and precursors for the most intense signals from the background ions for the different seasons.

Season	ID ¹	Formula	<i>m/z</i>	OSC	Possible identity	Precursor	Reference
WS18	a	C ₅ H ₁₂ O ₇ S	215.0231	-	IEPOX-OS	Isoprene	(Worton et al., 2013) (Kourtchev et al., 2016)
	b	C ₅ H ₆ O ₄	129.0194	0.4	Dicarboxylic acid / Peroxy acid	Methylfuran	(Joo et al., 2019)
	c	C ₅ H ₁₀ O ₅	149.0455	0.0	Carbonyl-tetrol / Epoxy-tetrol / Carboxyl-triol	Isoprene	(Krechmer et al., 2015) (Chen et al., 2020)
	d	C ₈ H ₁₂ O ₄	171.0662	-0.5	Ketolimonic acid / Terpenylic acid	Limonene / α - pinene	(Hammes et al., 2019) (Eddingsaas et al., 2012)
DS18	A	C ₅ H ₁₀ O ₅	149.0455	0.0		See ID c	
	B	C ₄ H ₆ O ₄	117.0193	0.5	Succinic acid	-	(Wang et al., 2017)
	C	C ₇ H ₁₀ O ₅	173.0454	0.0		α -pinene	(Chen et al., 2020) (Kleindienst et al., 2007)
	D	C ₄ H ₆ O ₅	133.0142	1.0	Malic acid	Isoprene	(Nguyen et al., 2010)

¹ IDs correspond to the labels illustrated in Figure 1.

3.2.2 Carbon oxidation states

365 To further characterize the background chemical composition of the aerosol, the average carbon oxidation state (OSC) was
 370 calculated for each detected molecular CHO formula. This metric was introduced by Kroll et al. (2011) and is a useful
 parameter to describe complex mixtures of organic aerosols. Various chemical and physicochemical processes in the
 atmosphere are determined by the oxidation state of the organic components. For example, highly oxidized molecules (HOM)
 with sufficiently low volatility can form ~~clusters~~ *clusters*, which leads to the formation of new particles and subsequent particle
 growth, even of small particles (Bianchi et al., 2016; Molteni et al., 2016).

To give an impression of the position of the corresponding OSC values within the regular Van Krevelen plots, organic
 compounds with OSC = 0 are indicated by the dashed line in [Figure- 14](#). To the left are compounds with an OSC <0 (not or
 less oxidized), to the right are compounds with OSC values > 0, e.g. the HOMs, which are defined as molecules with O/C \geq
 0.6 and/or OSC \geq 0 (Tu et al., 2016). As shown in [Figure- 1](#), the samples from the 2018 dry season had the highest number of
 375 highly oxidized compounds, which accounted for about 30 % of the total number of compounds. The average molecular
 formula for the HOMs in the 2018 dry season was C_{6.5}H_{8.6}O_{5.1} with C₄-C₁₀ backbones, which can be interpreted that
 isoprene and monoterpene precursors are also the main source of HOMs in the Amazon rainforest in the dry season. The 2019
 dry season showed fewer oxidized molecules, with a mean molecular formula of C_{6.7}H_{10.2}O_{5.7}. [The difference in HOM
 concentrations between the dry seasons of 2018 and 2019 may be related to differences in the chemical composition of OH
 reactivity during those periods. Pfannerstill et al. \(2020\) observed that while total OH reactivity was higher in September 2019
 380 than in October 2018 \(29.1 \$\pm\$ 10.8 s⁻¹ vs. 28.1 \$\pm\$ 7.9 s⁻¹ at 80 m\), this increase was not driven by monoterpenes, which are key
 precursors for HOM formation. The high OH reactivity in the dry season 2019 was rather dominated by oxidized VOCs, such
 as aldehydes and organic acids. This shift toward more oxidized and aged VOCs indicates a more photochemically processed](#)

385 air mass, potentially affected by biomass burning. Although NO_x was not measured (Figure S8), the authors suggest that fire-
390 related emissions may have altered the oxidation regime. Given that high NO_x levels can suppress RO₂ autoxidation and
thereby inhibit HOM formation, and that monoterpene contributions to OH reactivity were not elevated in 2019, it is plausible
that the observed reduction in HOMs was due to a combination of reduced precursor availability and a shift in chemical
conditions unfavorable for HOM production.

-However, it should be noted that the analysis of highly oxygenated compounds would benefit from the use of a more polar
stationary phase of the LC column, as a more comprehensive analysis of analytes of the entire polarity range would be enabled.
This would ensure that even the very polar species are not underestimated due to insufficient separation.

Figure 2 shows the OSC values as a function of carbon number for each CHO compound, with OSC values ranging from -1.5
to +1.2 in the dry seasons and from -1.1 to +1.0 in the wet seasons. This result is consistent with other studies in remote
continental areas (Kourtchev et al., 2013; Kourtchev et al., 2016). Molecules with an OSC between -0.5 and -1.5 and a carbon
number greater than seven are considered biomass-burning organic aerosol (BBOA). The comparison between dry and wet
seasons clearly shows the large number of compounds associated with BBOA and that these substances contribute substantially
to the SOA load of the Amazon rainforest during dry seasons. Interestingly, the contribution of BBOA-related compounds was
significantly higher in the 2019 wet season (Figure S 129), which is likely due to the increased number of active fires during
this period. In contrast, molecules with an OSC between -0.5 and +1.0 and less than 13 carbon atoms are generally associated
with semivolatile and low-volatility oxygenated organic aerosol (SV-OOA and LV-OOA) (Kroll et al., 2011; Wang et al.,
2017). These compounds are formed by multiple oxidation reactions and are commonly attributed to fresh and aged SOA,
respectively (Zhang et al., 2007; Jimenez et al., 2009). The background chemical composition during the dry seasons also
revealed numerous compounds attributed to LV-OOA indicating more aged SOA components compared to the wet seasons.

Whether the lower precipitation in the dry season and the associated longer residence times of the OA in the atmosphere are
the cause of these observations, or whether these compounds also have their source in biomass combustion processes, cannot
be clearly determined here. In contrast, the majority of background compounds during rainy seasons are associated with SV-
OOA, suggesting that local biogenic emissions are the main source of freshly formed SOA. Overall, Figure 2 clearly shows
that large differences in chemical composition exist between the two seasons in the Amazon rainforest. ~~However, we did not~~
observe significant variations at different altitudes.

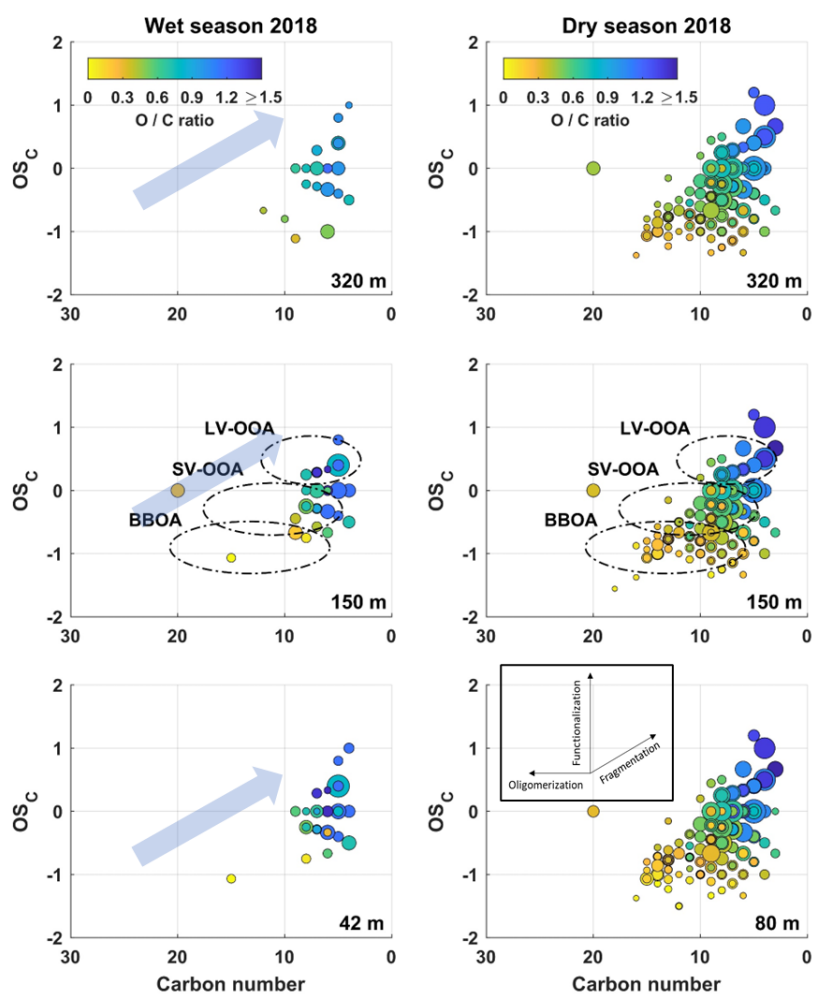


Figure 2: Carbon oxidation state (OSC) plots for all detected CHO species during the wet season 2018 (left) and dry season 2018 (right) at different sampling heights. Only background ions are included. The size of the data points represents the signal intensity of the corresponding peak. The color code illustrates the degree of oxygenation. The black dashed areas are related to low-volatility (LV-OOA) and semivolatile (SV-OOA) oxygenated organic aerosol and biomass-burning organic aerosol (BBOA). Insets: vectors corresponding to key classes of reactions of atmospheric organics: functionalization (addition of polar functional groups), fragmentation (cleavage of C–C bonds), and oligomerization (covalent association of two organic species). The combination of these reaction types leads to complex movement through (–the OSC–carbon number–) space; however, the inevitable increase in OSC with atmospheric oxidation implies that, given enough time, organics will generally move up and to the right (blue arrows). Insets based on Kroll et al., 2011.

3.2.3 Height-dependency of the background OA characteristics

The vertical profiles of the background organic aerosol (OA) composition exhibited only subtle variations across the sampled heights, with much smaller gradients than those observed between seasons. As illustrated in the van Krevelen diagrams (Figure 1) and summarized in Table S2, the background OA was dominated by CHO-type compounds at all heights and during all seasons, accounting for 82 % to 98 % of the detected molecular formulas. Nitrogen- and sulfur-containing species (CHON,

hat formatiert: Schriftart: 10 Pt., Nicht Fett, Englisch (Vereinigtes Königreich)

hat formatiert: Schriftart: 10 Pt., Nicht Fett, Englisch (Vereinigtes Königreich)

3.3 Variable OA characteristics

The occurrence of variable component contributions to the chemical composition of OA is attributed to irregular atmospheric events, which are presumably caused by varying meteorological conditions, i.e. uncommon wind direction, long-range transported plumes or fires or anthropogenic pollution nearby. Compounds that were only detected once in the respective data set were excluded, as they were not considered representative. As already mentioned, the previously discussed background compounds were not taken into account for the group of variable compounds defined here. The remaining signals were assigned according to the sampling time during the day (7:00 - 17:00 local time, UTC-4 h) and night (17:00 - 7:00 local time, UTC-4 h). An additional sample in the morning (7:00 – 12:00 local time, UTC-4 h) was collected during the dry season 2019 only, while the daytime sample was collected between 12:00 and 17:00 local time, UTC-4 h. The results and trends for 2018 and 2019 are discussed in this chapter, are considered representative for both years (2018 and 2019) but and for clarity, the graphs for 2019 are shown in the supplement (Figure S 13-16!, Figure S 12).

3.3.1 Molecular tracer compounds of individual events

In this section, Van Krevelen and OSC diagrams are discussed with the aim of identifying molecular tracer components that can be associated with individual meteorological or atmospheric chemical events. Representative VK diagrams for the seasons in 2018 are shown in Figure 3. The respective diagrams of the wet and dry season 2019 are shown in Figure S13 and S14.

With the non-targeted approach used in this study, only small altitude dependent differences in the chemical composition of OA could be observed. Therefore, only VK diagrams of samples at 320 m altitude are discussed in this section. For better understanding, the VK diagrams were divided into five areas: *I* for very highly oxidized organic compounds, *II* for highly oxidized compounds, *III* for intermediately oxidized compounds, *IV* for oxidized unsaturated organic compounds and *V* for highly unsaturated organic compounds. The five areas were defined according to Zhang et al., -2021.

(I) Very highly oxidized organic compounds: Area I shows very highly oxidized organic compounds, with isoprene oxidation products being a distinctive feature. Since less wet deposition of aerosol particles occurred due to less precipitation events during the dry season 2018, a greater number of compounds were identified during the dry season 2018 than during the wet season 2018. This result is consistent with the particle mass and number concentrations (Figure S 64, Figure S 75) observed during these campaigns.

No significant differences were observed for the corresponding daytime and nighttime samples for the wet season 2018. $C_5H_{12}O_4$ (m/z 136.0662) was detected in all samples from all seasons and identified as 2-methyltetrole, a prominent product of isoprene oxidation (Claeys et al., 2004). A large number of CHOS compounds were detected during the dry season 2018. More than 85 % of the CHOS molecules detected showed an O/S ratio ≥ 4 , indicating the presence of at least one sulfate functional group. Species with $O/C \geq 1$ and $H/C \geq 2$ with highly oxygenated C4 and C5 backbones were particularly prominent. Their structures emphasize that isoprene is the main precursor for S-containing OA at ATTO. $C_5H_{12}O_7S$ (m/z 215.0231, IEPOX-OS) and $C_5H_{10}O_7S$ (m/z 213.0075) were detected in filter samples from all four campaigns and showed the highest intensities. Both structures have already been identified as isoprene-derived OS and correlate with increased sulfate concentrations during dry periods. The latter can be attributed to the long-range transport of anthropogenic emissions (Andreae et al., 2015).

It is well established that isoprene-derived organosulfates are primarily formed via photochemical oxidation mechanisms, involving reactive intermediates such as ISOPOOH and IEPOX under low-NO conditions, often leading to enhanced production during the daytime (Surratt et al., 2007; Surratt et al., 2008). However, in our study, we observed consistently higher CHOS signal intensities at night across all seasons. While OS formation is photochemically driven, the nocturnal enhancement in signal intensities is likely not indicative of in situ nighttime production, but instead reflects more efficient partitioning into the particle phase during cooler nighttime conditions. This explanation is consistent with the findings of Gómez-González et al. (2012) and Kourchev et al. (2014b), who also reported strong diurnal differences driven by temperature-dependent gas-particle partitioning. In addition, higher CHOS signal intensities were observed in all nocturnal samples than in the corresponding daytime samples in the dry season 2018, which shows a pronounced diurnal variation and

efficient partitioning into the particle phase during cooler nighttime conditions. This explanation is consistent with the findings of Gómez-González et al. (2012) and Kourchev et al. (2014b), who also reported strong diurnal differences driven by temperature-dependent gas-particle partitioning. In addition, higher CHOS signal intensities were observed in all nocturnal samples than in the corresponding daytime samples in the dry season 2018, which shows a pronounced diurnal variation and

hat formatiert: Schriftfarbe: Text 1, Englisch (Vereinigtes Königreich)

hat formatiert: Englisch (Vereinigtes Königreich), Nicht Hervorheben

hat formatiert: Englisch (Vereinigtes Königreich), Nicht Hervorheben

hat formatiert: Englisch (Vereinigtes Königreich), Nicht Hervorheben

hat formatiert: Schriftart: Nicht Fett

hat formatiert: Schriftfarbe: Text 1

hat formatiert: Nicht Hervorheben

hat formatiert: Nicht Hervorheben

hat formatiert: Schriftfarbe: Text 1

hat formatiert: Schriftfarbe: Text 1

can be explained by the temperature dependence of gas-particle partitioning (Kourtehev et al., 2014b; Gómez-González et al., 2012).

Concerning the height-dependent analysis the wet season 2018 reveals that CHON and CHOS species in area I were more abundant at 42 m (slightly above canopy) during the day, whereas their number increased at 320 m during the night. CHO compounds, in contrast, showed a lower relative contribution at 320 m compared to 42 m in both, day and night samples. (Fig 3). These observations suggest a vertical redistribution of specific compound classes influenced by boundary layer dynamics. The nocturnal increase in CHON and CHOS compounds aloft may be related to residual layer effects or long-range transport, whereas the canopy-level daytime maxima point to local, biogenic emissions and in-canopy photochemical processing. In the dry season 2018, no clear vertical trend was observed in area I, suggesting enhanced atmospheric mixing and a more homogeneous chemical distribution due to convective processes. These interpretations are supported by recent findings that showed that under very stable nocturnal conditions (assumed for wet season 2018), the boundary layer height can remain below 100 m, allowing upper levels (e.g., 320 m) to remain decoupled and enriched in aged or transported aerosol components. Furthermore, the prevalent southwesterly wind direction in the dry season 2018 is associated with higher surface roughness and increased turbulence, potentially leading to more uniform vertical distributions and mixing of aged, oxidized species (Mendonca et al., 2025).

(II) Highly oxidized organic compounds: In general, area II is characterized by highly oxidized organic species, like late monoterpene oxidation products due to oxidative aging or higher generation oxidation products (Zhang et al., 2021). The dry season 2018 shows a higher number of compounds than the wet season 2018, indicating more aged organic aerosol. This is also underlined by an increased number of LV-OOA species in the OSC plots in Figure 4. An intense ion signal with m/z 203.0562 ($C_8H_{12}O_6$) could be assigned to 3-methyl-1,2,3-butanetricarboxylic acid (MBTCA) by comparison with an authentic standard (Table S5). MBTCA is a well-established tracer compound for aged biogenic SOA formed by the photooxidation of α - and β -pinene (Szmigielski et al., 2007; Zhang et al., 2010). Similarly, two detected CHONS compounds at m/z 294.0654 ($C_{10}H_{17}O_7NS$) and m/z 296.0446 ($C_9H_{15}O_8NS$) were associated with aged SOA, which were previously identified as oxidation products of α -pinene, β -pinene and limonene (Surratt et al., 2008). The O/(N+S) ratio ≥ 3.5 allows for the presence of both -OSO₂H and -ONO₂ functional groups and assignment as nitrooxy organosulfates (NOS). Similar to the higher concentrations of very highly oxidized CHOS species (I), highly oxidized (II) CHONS species also show increased concentrations in dry periods and high correlations with SO₂ levels, but also NO_x concentrations (increased NO_x and black carbon equivalent concentrations (BCe) in the dry season 2018; Figure S86 and S173). This underlines the importance of anthropogenic emissions reaching the ATTO site by long-distance transport and changing the chemical composition of organic aerosols by mixing biogenic and anthropogenic sources.

The molecular assignment of two further ions, m/z 161.0455 ($C_6H_{10}O_3$) and m/z 129.0194 ($C_5H_6O_4$) with increased concentrations in the dry season clearly shows a connection with biomass burning activities. The overall burning activity in the basin was significantly lower in the wet season 2018 compared to the dry season 2018 (Table S 3). $C_6H_{10}O_3$ can be assigned to 1,6-anhydro- β -D-glucopyranose (Levoglucosan) by comparison with authentic standard substances (Table S5). Levoglucosan is a generally recognized product of cellulose pyrolysis that is used as a marker compound for biomass burning activities (Simoneit et al., 1999; Nolte et al., 2001). However, $C_5H_6O_4$ can be explained less clearly. A compound with this molecular formula was found as an oxidation product of the reaction of 3-methylfuran with NO₃ radicals (Joo et al., 2019), while furans themselves were detected as products of cellulose combustion (Mettler et al., 2012). The $C_5H_6O_4$ molecule observed here showed higher concentrations in dry season samples (higher number of fires) and in night samples (nitrate radical chemistry), supporting the hypothesis that the reaction of 3-methylfuran with NO₃ radicals is a source of this compound.

hat formatiert: Schriftart: Nicht Kursiv, Schriftfarbe: Text 1, Englisch (Vereinigtes Königreich)

hat formatiert: Schriftfarbe: Text 1

hat formatiert: Schriftfarbe: Text 1, Englisch (Vereinigtes Königreich)

hat formatiert: Schriftart: Nicht Kursiv, Schriftfarbe: Text 1, Englisch (Vereinigtes Königreich)

hat formatiert: Schriftfarbe: Text 1

hat formatiert: Schriftart: Nicht Kursiv, Schriftfarbe: Text 1, Englisch (Vereinigtes Königreich)

hat formatiert: Schriftfarbe: Text 1

hat formatiert: Schriftart: Nicht Kursiv, Schriftfarbe: Text 1, Englisch (Vereinigtes Königreich)

hat formatiert: Schriftfarbe: Text 1, Englisch (Vereinigtes Königreich)

hat formatiert: Schriftart: Nicht Kursiv, Schriftfarbe: Text 1, Englisch (Vereinigtes Königreich)

hat formatiert: Schriftfarbe: Text 1

hat formatiert: Schriftart: Nicht Kursiv, Schriftfarbe: Text 1, Englisch (Vereinigtes Königreich)

hat formatiert: Schriftart: Nicht Fett

hat formatiert: Tiefgestellt

hat formatiert: Tiefgestellt

hat formatiert: Schriftart: Nicht Fett

hat formatiert: Schriftart: Nicht Fett

hat formatiert: Tiefgestellt

hat formatiert: Tiefgestellt

hat formatiert: Nicht Hervorheben

hat formatiert: Nicht Hervorheben

hat formatiert: Schriftart: Nicht Fett

hat formatiert: Schriftart: Nicht Fett

hat formatiert: Schriftart: Nicht Fett, Kursiv, Deutsch (Deutschland)

hat formatiert: Schriftfarbe: Text 1

However, the C5 backbone can also suggest isoprene as potential precursor, which can also form C₅H₈O₄ according to photooxidation experiments in chamber studies (Nguyen et al., 2011; Clark et al., 2013).

During the wet season 2018, the oxidized organic aerosol subtype LV-OOA showed its highest O/C ratios at 150 m during daytime (Fig 4), indicating a vertical gradient in oxidation state. While the oxidation state increased with height, the total number of LV-OOA species decreased at 320 m. This pattern is consistent with oxidative aging during vertical transport and lower precursor availability aloft. At night, this vertical pattern persisted, albeit with overall lower O/C ratios. CHON signals in area II were most abundant at 320 m, leading to the assumption that highly oxidized, aged CHON compounds reached the ATTO site by long-range transported aerosols.

(III) Intermediately oxidized organic compounds: Area III mostly consists of first-generation oxidation products of monoterpenes and sesquiterpenes that are intermediately oxidized (Zhang et al., 2021). Again, the dry season 2018 is characterized by a higher number and concentration of compounds than the wet season 2018 while no significant differences are observed between the daytime and nighttime samples. The compounds are characterized by aliphatic species that can be attributed to mixed anthropogenic and biogenic sources (Henze et al., 2008; Kourtev et al., 2013). A prominent ion was observed at *m/z* 185.0819, which was assigned to the molecular formula C₉H₁₄O₄. The compounds with this molecular formula showed multiple signals in the LC-MS analysis, indicating the presence of several isomeric structures. One signal was identified as pinic acid (PA) from an authentic standard compound (Table S5). The additional signals are likely to be oxidation products of other monoterpenes, such as β-pinene, limonene and Δ³-carene (Jenkin, 2004; Chen and Griffin, 2005; Hammes et al., 2019). In contrast to MBTCA, pinic acid is an oxidation product that is already formed during the first oxidation steps of α-pinene and can therefore be used as a tracer for freshly formed SOA. Later generation products, such as MBTCA, were more concentrated in the dry seasons, indicating more processed SOA particles, while PA was predominant in the wet periods. The OSC analysis in Figure 4 shows that the dry season 2018 has pronounced signals at small numbers of C atoms with high O/C ratios, whereas the wet season 2018 is characterized by pronounced SV-OOA species, supporting the different seasonal variation of different generations.

During the wet season 2018, CHO and CHON species in area III were most abundant at 42 m during daytime, indicating a dominant contribution from local biogenic sources within or just above the canopy. CHO compounds decreased with height, while CHON compounds remained relatively constant (Fig 3). At night, however, CHON signals dropped at 42 m, possibly due to suppressed vertical mixing or altered chemical production pathways. This suggests that canopy dynamics and photochemical activity strongly influence the vertical distribution of first-generation monoterpene oxidation products. These trends are consistent with the findings of Mendonça et al. (2025), which indicate that under wet season conditions, when the wind predominantly arrives from the northeast (Fig S5) and the surface roughness is relatively low, the nocturnal boundary layer is shallow (typically 80–120 m), limiting vertical exchange and favoring accumulation of semivolatile species near the canopy top.

(IV) Oxidized unsaturated organic compounds: This area is mainly characterized by unsaturated hydrocarbons with a low oxygen content. Most of these compounds are classified as CHON, CHOS and CHONS with X_c ≥ 2.5, indicating aromatic molecular structures. The dry season 2018 shows a higher diversity of compounds whereas the wet season 2018 consists of a lower number of compounds mainly dominated by CHO species. At nighttime during the wet season 2018, the concentrations of CHO compounds are reduced. In contrast, the nighttime samples from the dry season 2018 do not exhibit a similar trend in concentrations. However, the drywet season of 2018 shows a higher presence of CHON species during nighttime compared to daytime samples. The most intense ion signals in the dry season 2018 *m/z* 154.0146 (C₆H₅NO₄, 4-nitrocatechol), *m/z* 168.0301 (C₇H₇NO₄, methyl-nitrocatechols) and *m/z* 185.0457 (C₈H₉NO₄, dimethyl-nitrocatechols) can be associated with nitroaromatic compounds, which are also considered markers for biomass burning OA (Iinuma et al, 2010; Claeys et al, 2012; Kitanovski et

hat formatiert: Schriftart: Nicht Kursiv, Englisch (Vereinigte Staaten)

hat formatiert: Schriftart: Nicht Kursiv, Englisch (Vereinigtes Königreich)

hat formatiert: Schriftfarbe: Text 1

hat formatiert: Schriftart: Nicht Kursiv, Englisch (Vereinigtes Königreich)

hat formatiert: Schriftfarbe: Text 1

hat formatiert: Schriftart: Nicht Kursiv, Englisch (Vereinigtes Königreich)

hat formatiert: Schriftfarbe: Text 1

hat formatiert: Schriftart: Nicht Kursiv, Englisch (Vereinigtes Königreich)

hat formatiert: Englisch (Vereinigtes Königreich)

hat formatiert: Schriftart: Nicht Kursiv, Englisch (Vereinigtes Königreich)

hat formatiert: Schriftfarbe: Text 1

hat formatiert: Schriftart: Nicht Kursiv, Englisch (Vereinigtes Königreich)

hat formatiert: Schriftfarbe: Text 1

hat formatiert: Schriftart: Nicht Kursiv, Englisch (Vereinigtes Königreich)

hat formatiert: Schriftart: Nicht Fett

hat formatiert: Schriftart: Nicht Fett

hat formatiert: Schriftart: Nicht Fett

hat formatiert: Schriftart: Nicht Kursiv, Englisch (Vereinigte Staaten)

hat formatiert: Schriftart: Nicht Kursiv, Englisch (Vereinigtes Königreich)

hat formatiert: Englisch (Vereinigtes Königreich)

hat formatiert: Schriftart: Nicht Kursiv, Englisch (Vereinigtes Königreich)

hat formatiert: Schriftfarbe: Text 1

hat formatiert: Schriftart: Nicht Kursiv, Englisch (Vereinigtes Königreich)

hat formatiert: Schriftfarbe: Text 1

hat formatiert: Schriftart: Nicht Kursiv, Englisch (Vereinigtes Königreich)

hat formatiert: Schriftfarbe: Text 1

hat formatiert: Schriftart: Nicht Kursiv, Englisch (Vereinigtes Königreich)

hat formatiert: Schriftfarbe: Text 1

hat formatiert: Schriftart: Nicht Kursiv, Englisch (Vereinigtes Königreich)

hat formatiert: Schriftart: Nicht Fett, Englisch (Vereinigtes Königreich)

hat formatiert: Schriftart: Nicht Fett

hat formatiert: Schriftart: Nicht Fett

hat formatiert: Nicht Hervorheben

al, 2012; Kahnt et al, 2013; Siemens et al., 2023). Kourtchev and coworkers (Kourtchev et al., 2016) also observed elevated concentrations of these compounds in the Amazon region during the period when numerous forest fires occurred. In contrast, no nitrocatechols were detected for the wet season 2018. However, C₆H₅NO₄ was the only compound identified as a background species during the dry season 2018 (Figure 1), suggesting a lower SOA contribution from C₇H₇NO₄ and C₈H₉NO₄ at ATTO.

Vertically resolved analysis of the wet season 2018 revealed that CHO signals in area *II* were less abundant at 320 m compared to lower levels, similar as described in area *III*. No significant day-night differences were observed, indicating that these compounds may be governed more by long-range transport and vertical diffusion than by in situ photochemistry. The lack of clear diurnal variation points to a more persistent source, possibly influenced by combustion-related emissions or stabilized air masses.

I) Highly unsaturated organic compounds; Area *V* is predominantly composed of highly unsaturated organic compounds that are combustion-related (Zhang et al., 2021). The number of compounds and the variety of species is enhanced for the dry season 2018 compared to the wet season 2018. This trend is also reflected in the BBOA areas in Figure 4. Furthermore, black carbon equivalent concentrations (BCe) were enhanced during the dry season 2018 compared to the wet season 2018 (Figure S17). No single dominant species was identified among the combustion-related highly unsaturated organic compounds, as their composition varied substantially between seasons. While the wet season 2018 shows mainly CHO species with a decreased number of compounds concentrations during nighttime, the dry season 2018 is dominated by CHOS and CHONS species and an increased number of CHON compounds during nighttime, suggesting enhanced particle-phase partitioning at lower temperatures.

During the wet season 2018, a greater number of highly unsaturated compounds were detected at 42 m compared to 320 m, both day and night. This points to a near-surface deposition and limited vertical mixing under stable boundary layer conditions, whereas no significant height resolved differences were observed for the dry season 2018.

The wet season of 2019 stands out due to individual pollution events that significantly influenced aerosol composition at the ATTO site. The number of components and their intensity increase across areas *I–V* for the wet season 2019 (Figure S13), compared to the wet season 2018 (Figure 3) and the dry season of the same year (Figure S14). The wet season 2019 also shows higher levels of CHON and CHO species relative to the 2019 dry season. The concentrations of OS related to isoprene remain comparable to those observed during the dry seasons of 2019 and 2018. In particular, area *V* in Fig S13 and the BBOA area in Fig S15 highlight the impact of biomass burning during this period. This is further supported by elevated BCe concentrations (Fig S17). While the background OA characterization still shows typical wet season features, such as low BBOA contributions, a dominance of early-stage monoterpene oxidation products, minimal aging effects (Figure S12), and absent signals in area *V* (Figure S9), it becomes evident that, with the inclusion of individual events, episodes of considerable pollution were present, temporarily altering the aerosol profile. These deviations likely reflect enhanced fire or combustion activity upwind or near the ATTO site during this period (Table S3). Additionally, emissions from biomass burning in the Sahel savanna regions, transported across the Atlantic Ocean (Fig S5), could have contributed to the observed aerosol characteristics (Holanda et al., 2020; Holanda et al., 2023).

The wet season of 2019 stands out and emphasizes the influence of aerosol composition on ATTO through individual events. The number of components and their intensity are both increased in areas *I–V* for the wet season 2019 in comparison to the wet season 2018, as well as in comparison to the dry season 2019 (Figure S11). The wet season 2019 generally exhibits increased concentrations of CHON and CHO species in comparison to the dry season of the same year. The concentrations of OS related to isoprene are of a similar magnitude to those observed during the dry seasons of 2019 and 2018. In particular, area *V* in Figure S11 and the BBOA area in Figure S12 demonstrate that the wet season 2019 was significantly influenced by

hat formatiert: Englisch (Vereinigtes Königreich)

hat formatiert: Schriftfarbe: Text 1

hat formatiert: Englisch (Vereinigtes Königreich)

hat formatiert: Schriftart: Kursiv, Englisch (Vereinigtes Königreich)

hat formatiert: Englisch (Vereinigtes Königreich)

hat formatiert: Schriftfarbe: Text 1

hat formatiert: Schriftart: Kursiv, Schriftfarbe: Text 1

hat formatiert: Englisch (Vereinigtes Königreich)

hat formatiert: Schriftfarbe: Text 1

hat formatiert: Englisch (Vereinigtes Königreich)

hat formatiert: Schriftfarbe: Text 1

hat formatiert: Schriftart: Nicht Fett

hat formatiert: Schriftfarbe: Text 1

hat formatiert: Schriftart: Nicht Fett

hat formatiert: Nicht Hervorheben

hat formatiert: Schriftfarbe: Text 1

hat formatiert: Schriftfarbe: Text 1

hat formatiert: Schriftart: Nicht Kursiv, Englisch (Vereinigtes Königreich)

hat formatiert: Schriftfarbe: Text 1

hat formatiert: Schriftart: Nicht Kursiv, Englisch (Vereinigtes Königreich)

hat formatiert: Schriftart: Kursiv

hat formatiert: Schriftart: Kursiv

hat formatiert: Schriftart: Kursiv

biomass burning and combustion activities. This is also reflected by enhanced BC concentrations (Figure S11). While the background OA characterization still exhibits clear wet season characteristics (low concentration in the BBOA area, dominance of early monoterpene oxidation products, lower significance of aerosol aging effects in Figure S10 and missing signals in area *V* in Figure S7), it becomes evident that, with the inclusion of individual events, significantly polluted conditions in the wet season 2019 could be discerned, which markedly alter the aerosol composition. This atypical behavior suggests a substantial influence from intensified forest fires or combustion activities occurring either upwind of the ATTO site or in its vicinity in the wet season 2019 (Table S3). Additionally, emissions from biomass burning in the Sahel savanna regions, transported across the Atlantic Ocean (Figure S8), could have contributed to the observed aerosol characteristics (Holanda et al., 2020; Holanda et al., 2023). In the wet season 2019, no significant vertical trends were observed across areas *I–V*, indicating a well-mixed atmosphere, possibly due to convective activity or large-scale transport. However, the dry season 2019, which included sampling at three different times and at sub-canopy level (0 m), revealed unique patterns. SV-OOA and CHOS compounds in areas *I* and *II* peaked at 80 m during nighttime, consistent with gas-particle partitioning favored by cooler, stable layers above the canopy. CHON compounds were most abundant at 0 m and 80 m in the morning but diminished at 320 m. These patterns underline the importance of both vertical stratification and local chemical processing in modulating aerosol composition at different heights and times of day. Mendonça et al. (2025) noted that dry season nights at ATTO, characterized by southwesterly winds and enhanced surface roughness, can exhibit deeper but more turbulent boundary layers, allowing complex layering and submesoscale motions to form, which could explain the varied height-dependent signals observed in this campaign. Moreover, the presence of the highest CHOS and SV-OOA signals at 80 m during nighttime suggests a zone of active condensation and SOA formation just above the canopy, where gas-particle partitioning is favored by cooler and more stable stratification. The fact that CHON species were relatively suppressed at 320 m both during morning and daytime indicates limited upward transport of nitrogen-containing precursors or their rapid transformation near the surface. The chemical differences between 0 m and 80 m, particularly for CHON and CHO species in areas *II* and *III*, also suggest that in-canopy processes such as deposition, emissions, and light penetration significantly modulate chemical composition. Together, these observations highlight the sensitivity of nighttime aerosol chemistry to fine-scale vertical structure and suggest that sub-canopy and canopy-top levels may act as chemically distinct compartments in the nocturnal boundary layer during the dry season.

hat formatiert: Schriftart: Nicht Kursiv, Englisch (Vereinigtes Königreich)

hat formatiert: Englisch (Vereinigtes Königreich)

hat formatiert: Schriftart: Nicht Kursiv, Englisch (Vereinigtes Königreich)

hat formatiert: Schriftfarbe: Text 1

hat formatiert: Schriftart: Nicht Kursiv, Englisch (Vereinigtes Königreich)

hat formatiert: Englisch (Vereinigtes Königreich)

hat formatiert: Schriftart: Nicht Kursiv, Englisch (Vereinigtes Königreich)

hat formatiert: Englisch (Vereinigtes Königreich)

hat formatiert: Schriftart: Nicht Kursiv, Englisch (Vereinigtes Königreich)

hat formatiert: Englisch (Vereinigtes Königreich)

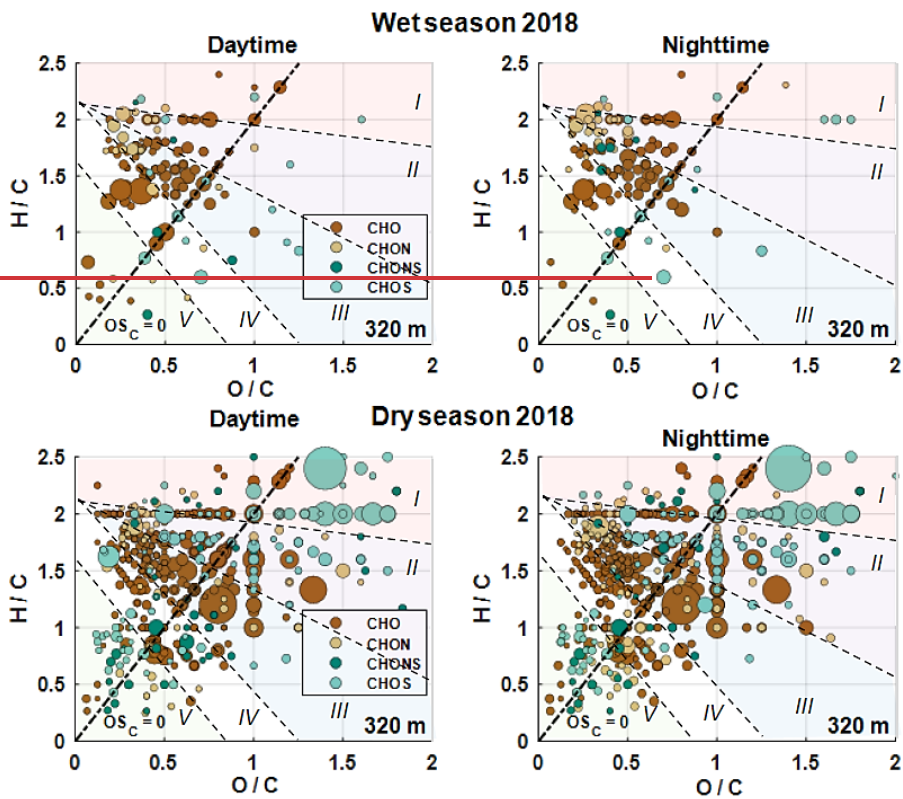
hat formatiert: Schriftart: Nicht Kursiv, Englisch (Vereinigtes Königreich)

hat formatiert: Schriftfarbe: Text 1

hat formatiert: Schriftfarbe: Text 1, Englisch (Vereinigtes Königreich)

hat formatiert: Schriftart: Nicht Kursiv, Englisch (Vereinigtes Königreich)

hat formatiert: Schriftfarbe: Text 1
hat formatiert: Englisch (Vereinigtes Königreich)



665

Formatiert: Nicht vom nächsten Absatz trennen

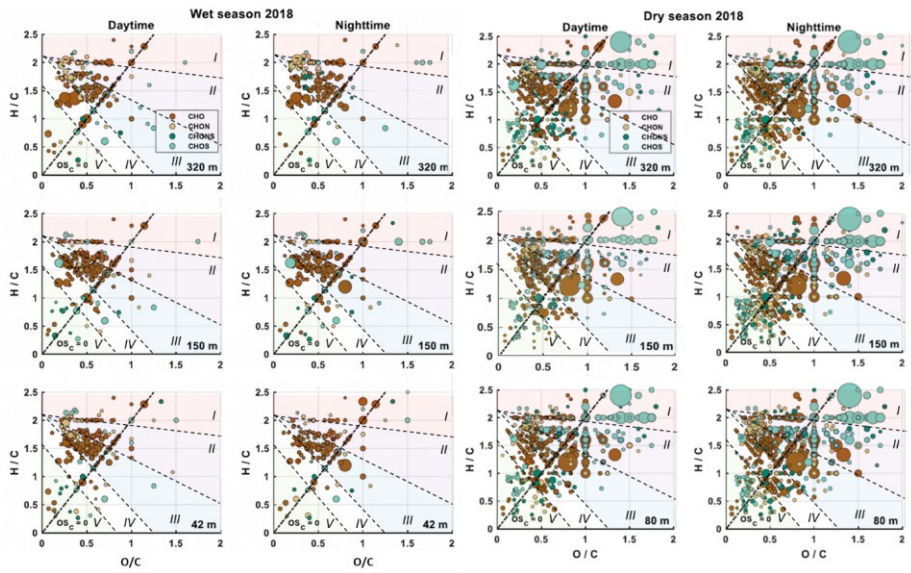


Figure 3: Van Krevelen-plots from the wet season 2018 (upper panel) and dry season 2018 (lower panel) during daytime (left

670 panel) and nighttime (right panel) at 320 m height. Included are only molecular formulae that were present in more than one
of the samples, respectively. The background signals are subtracted. The size of the data points represents the signal intensity
of the corresponding peak. The four subgroups CHO, CHON, CHONS and CHOS are distinguished with different colors.
675 Compounds located on the black dashed line have an average carbon oxidation state of 0 (OSC = 0). The VK diagram was
divided into five areas: I for very highly oxidized organic compounds, II for highly oxidized compounds, III for intermediately
oxidized compounds, IV for oxidized unsaturated organic compounds and V for highly unsaturated organic compounds. The
five areas were defined according to Zhang et al., 2021. Area (I) is mainly characterized by CHOS molecules with at least one
sulfate functional group and C4 and C5 backbones. Area (II) is dominated by highly oxidized compounds representing aged
OA and biomass burning products. Area (III) shows mainly aliphatic species. Area (IV) is dominated by unsaturated
hydrocarbons with low oxygen content and aromatic structures while area (V) shows mainly combustion related species.

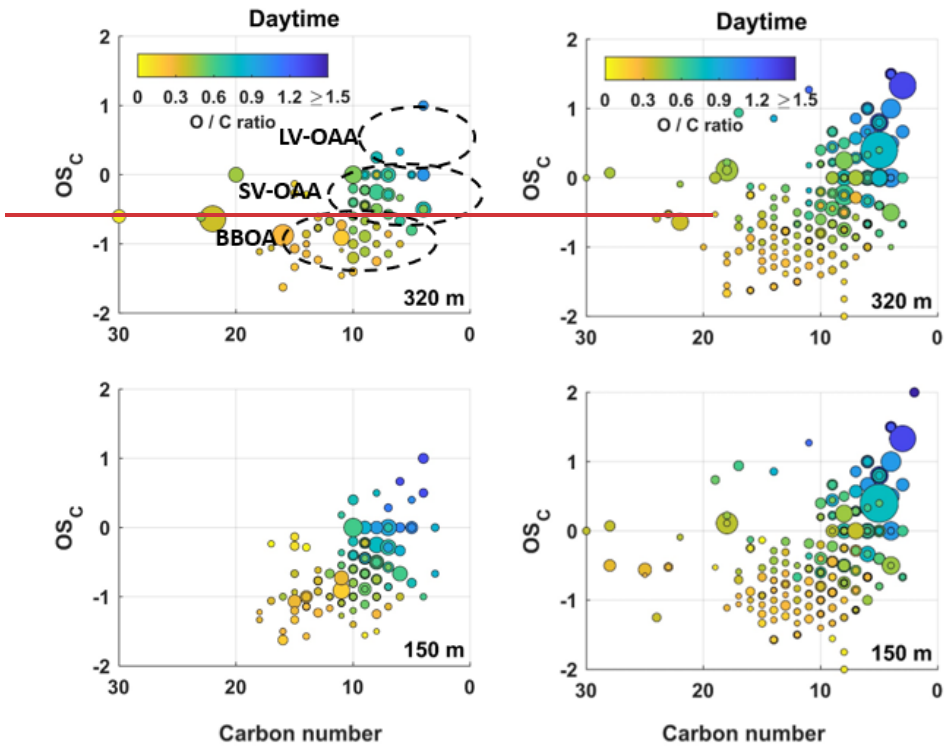
680 Figure 3: Van Krevelen plots from the wet season 2018 (left panel) and dry season 2018 (right panel) during daytime and nighttime
at 42 m, 150 m, 320 m height and 320 m height and dry season 2018 (right panel) during daytime and nighttime at 80 m, 150 m, and
320 m height. Included are only molecular formulae that were present in more than one of the samples, respectively. The background
signals are subtracted. The size of the data points represents the signal intensity of the corresponding peak. The four subgroups
685 CHO, CHON, CHONS and CHOS are distinguished with different colors. Compounds located on the black dashed line have an
average carbon oxidation state of 0 (OSC = 0). The VK diagram was divided into five areas: I for very highly oxidized organic
compounds, II for highly oxidized compounds, III for intermediately oxidized compounds, IV for oxidized unsaturated organic
compounds and V for highly unsaturated organic compounds. The five areas were defined according to Zhang et al., 2021. Area (I)
is mainly characterized by CHOS molecules with at least one sulfate functional group and C4 and C5 backbones. Area (II) is
dominated by highly oxidized compounds representing aged OA and biomass burning products. Area (III) shows mainly aliphatic
species. Area (IV) is dominated by unsaturated hydrocarbons with low oxygen content and aromatic structures while area (V) shows
mainly combustion related species.

hat formatiert: Schriftfarbe: Text 1

hat formatiert: Schriftfarbe: Text 1

Wet season 2018

Dry season 2018



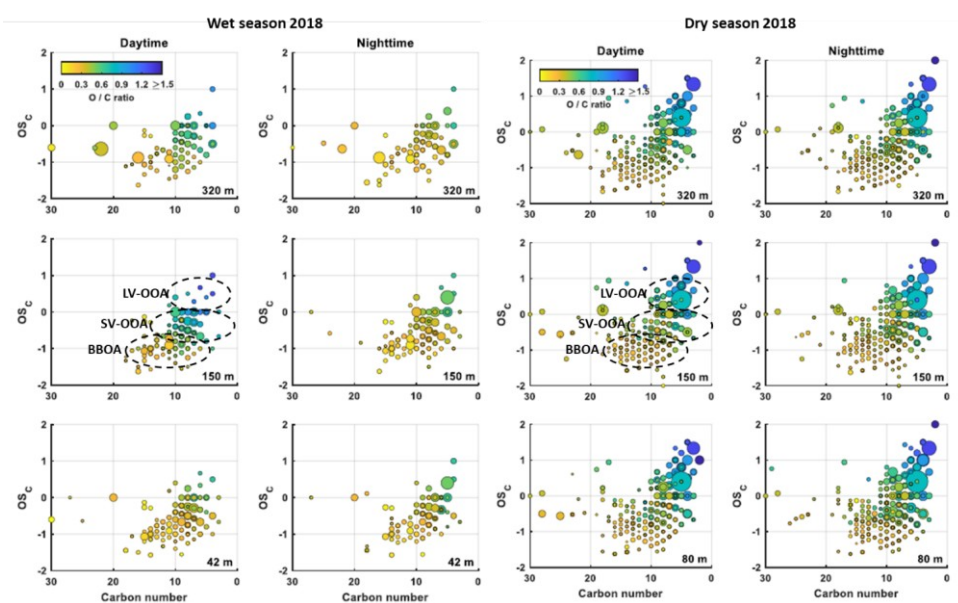


Figure 4: Carbon oxidation state (OSC) plots for all detected CHO species during the wet season 2018 at daytime (left) and dry season 2018 (right) at daytime at 150 m and 320 m sampling height. Included are only molecular formulae that were present in more than one of the samples, respectively. The background signals are subtracted. The size of the data points represents the signal intensity of the corresponding peak. The color code illustrates the degree of oxygenation. The black dashed areas are related to low-volatility (LV-OOA), semivolatile (SV-OOA) oxygenated organic aerosol and biomass burning organic aerosol (BBOA).

Figure 4: Carbon oxidation state (OSC) plots for all detected CHO species during the wet season 2018 at daytime and nighttime at 42 m, 150 m, 320 m and dry season 2018 (right) at daytime and nighttime at 80 m, 150 m and 320 m sampling height. Included are only molecular formulae that were present in more than one of the samples, respectively. The background signals are subtracted. The size of the data points represents the signal intensity of the corresponding peak. The color code illustrates the degree of oxygenation. The black dashed areas are related to low-volatility (LV-OOA), semivolatile (SV-OOA) oxygenated organic aerosol and biomass burning organic aerosol (BBOA).

3.3.2 Saturation vapor pressure

The saturation vapor pressure C^0 is an important thermodynamic property that regulates the gas-to-particle partitioning properties of organic molecules and enables their classification as VOCs, intermediate volatile organic compounds (IVOCs), semi-volatile OCs (SVOCs), low-volatility OCs (LVOCs) and extremely low-volatility OCs (ELVOCs) (Pankow, 1994; Odum et al., 1996; Murphy et al., 2014). The relationship between molecular weight, chemical composition and saturation vapor pressure has already been used to describe the chemical evolution of organic aerosols (Shiraiwa et al., 2014; Li et al., 2016). A case study Figure 5 compares 2-D maps of molecular weight plotted against saturation vapor pressure for the organic species observed in measured in this study from the dry and wet season 2018 is presented in Figure 5 showing 2-D maps of molecular weight versus saturation vapor pressure. Nearly all CHONS compounds are located within the LVOC/ELVOC range, and it is clear that many of the additional compounds detected occurring in the dry season exhibit have very low volatility, indicated by high molecular weights on the one hand, and a more oxidized (aged) character relative compared to the wet season composition on the other. Increased nitrogen oxide and SO_2 concentrations and thus the formation of N- and S-functionalized oxidation products, but also a lower removal by precipitation and thus longer residence times in the atmosphere could explain these differences between wet and dry season. These factors The seasonal difference suggest that the observed compounds

Formatiert: Nicht vom nächsten Absatz trennen

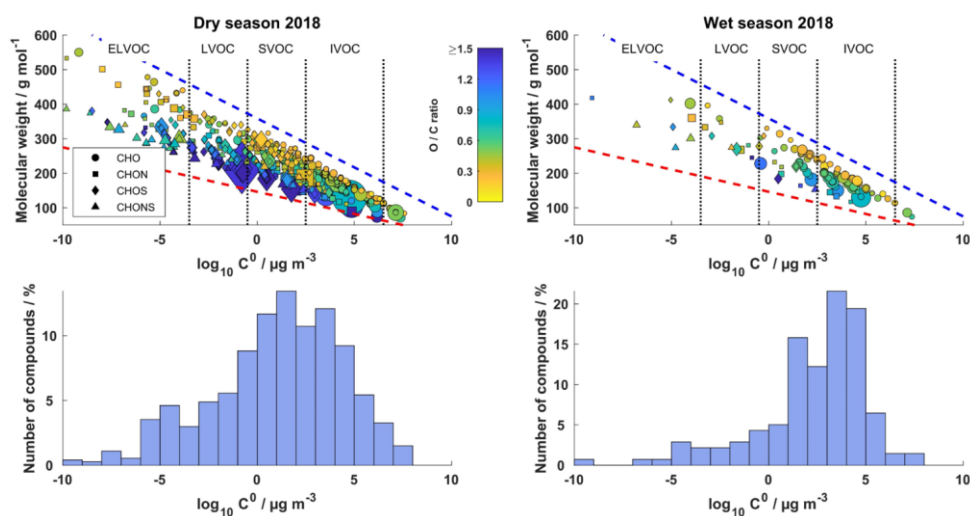
hat formatiert: Schriftfarbe: Text 1

hat formatiert: Schriftart: Fett

720 ~~reflect a regional they are part of the hemispheric wide~~ burning signature in the dry season. Several high molecular weight compounds with C8-C10 or C17-C20 backbones have also been identified as LVOC/ELVOC, suggesting oligomeric structures ~~derived from based on~~ isoprene and monoterpene precursors. It is hypothesized that these products are low volatile due to the incorporation of additional functional groups and the increase in carbon number in the molecular structure (Kroll and Seinfeld, 2008; Daumit et al., 2013). Two prominent ion signals at m/z 333.0859 ($C_{10}H_{22}O_{10}S$) and m/z 357.1557 ($C_{17}H_{26}O_8$) ~~were previously reported have already been observed~~ in chamber studies with isoprene and α -pinene (Surratt et al., 2008; Kristensen et al., 2013). ~~Most oligomers were detected in filter samples collected during the dry season, suggesting a stronger contribution of the oligomerization reaction to SOA under these conditions.~~ In addition to ~~oligomeric~~ structures derived from isoprene and monoterpene precursors, compounds with molecular formulae such as the $C_{14-15}H_{22-24}O_{3-7}$ were detected in the dry season 2018 (i.e. $C_{14}H_{22}O_3$; $C_{15}H_{24}O_4$), contributing to the LVOC fraction. ~~highest molecular weight (MW) of $500 < MW < 600$ g/mol were also found in the dry season 2018.~~ These signals ~~could are in line with indicate~~ oxygenated dimers of sesquiterpene oxidation products previously identified in chamber simulation experiments ~~offrom~~ β -caryophyllene ozonolysis (Gao et al., 2022) and could be assigned to β -caryophyllonic acid ($C_{15}H_{24}O_6$) as well as β -nocaryophyllonic acid and β -caryophyllinic acid ($C_{14}H_{22}O_6$) by comparison with authentic standard compounds (Table S5). The authors investigated the formation of SOA ~~under varying in the presence and absence of~~ nitrogen oxide levels at different temperatures. At a temperature of 313 K and the absence of nitrogen oxides, monomers (mainly $C_{14-15}H_{22-24}O_{3-7}$) and dimers (mainly $C_{28-30}H_{44-48}O_{5-9}$) could be detected. In the presence of nitrogen oxides, which is more ~~in line with the dry season 2018 conditions,~~ most organonitrates were found as ~~monomers with a C15 skeleton with characteristic of the dry season conditions in 2018, most organonitrates were found as monomers with a C15 skeleton and one a~~ nitrate group ($C_{15}H_{23-25}O_{7-9}N$). However, in the wet and dry season 2018 no significant contribution of $C_{28-30}H_{44-48}O_{5-9}$ or $C_{15}H_{23-25}O_{7-9}N$ could be found. In case of CHON compounds with only one N atom, the dominant compound in the dry season 2018 was $C_{14}H_{27}NO_7$. This molecule has previously been identified as a product of toluene-derived SOA in chamber experiments (Zhang et al., 2020). These findings imply that, in addition to biogenic precursors, aromatic anthropogenic emissions may also play a relevant role in shaping the low-volatility organic aerosol composition during the dry season. ~~Nevertheless, purely organic species without nitrogen atoms (C20, C35) were newly formed in the presence of nitrogen oxides, supporting the results presented here. Most oligomers were detected in filter samples from dry season campaigns, suggesting a stronger contribution of the oligomerization reaction to SOA during these periods.~~

745 ~~highest molecular weight (MW) of $500 < MW < 600$ g/mol were also found in the dry season 2018. These trends indicate that SOA formation and reactions make a greater contribution to ELVOC species during the dry seasons than during the wet seasons.~~

hat formatiert: Tiefgestellt



750 Figure 5: Molecular classification of organic species for the dry season 2018 (left) and the wet season 2018 (right) according to their saturation vapor pressure C^0 . The color code describes the degree of oxygenation. The blue dashed line indicates linear alkanes C_nH_{2n+2} , while the red dashed line represents sugar alcohols $C_nH_{2n+2}O_n$ according to Li et al. (2016). The lower panel shows the distribution of all detected compounds among the respective classes.

3.3.3 Kendrick mass analysis

755 Kendrick mass analysis is a valuable visualization tool for complex organic mixtures and was introduced by Kendrick (1963) and later refined by Hughey et al. (2001). This technique has already been used to characterize organic aerosol samples (Lin et al., 2012; Rincón et al., 2012; Kourtechev et al., 2013). It enables the assignment of all signals of a homologous series when the elemental composition of a compound has been identified (Nizkorodov et al., 2011). Figure 6 compares the KMD_{CH_2} diagrams (see eq. 2.5 and 2.6) for the dry and wet seasons in 2018. Compounds differing only in their number of CH_2 units

760 have the same KMD values. Homologous series can be identified as horizontal lines in KMD plots.

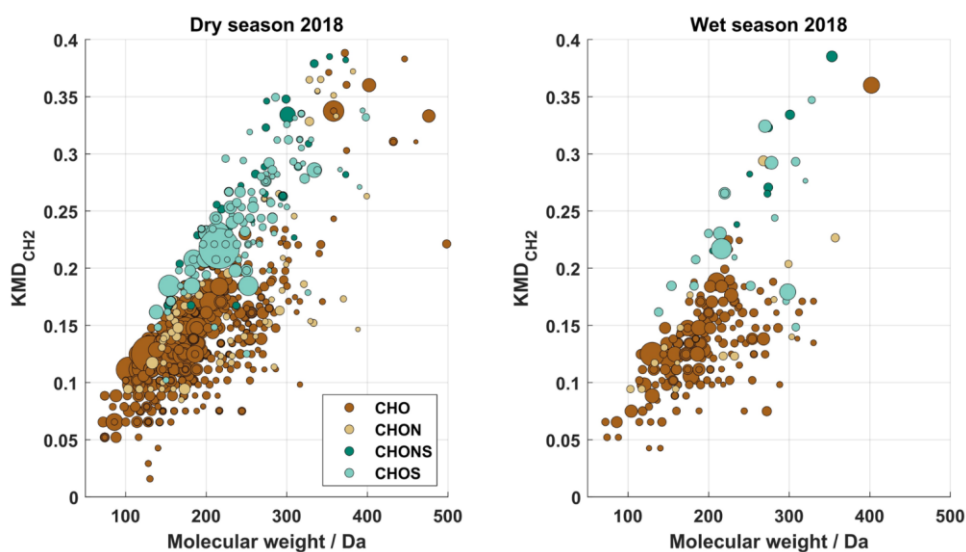


Figure 6: CH₂-Kendrick diagrams for all signals detected at 150 m during the dry season 2018 (left) and the wet season 2018 (right), respectively. The size of the data points represents the signal intensity of the corresponding peak. The four subgroups are distinguished with different colors.

765 As mentioned above, the dry season was characterized by biomass burning and the occurrence of aged organic aerosol components, resulting in large-membered homologous series of CHO compounds with higher MW than in the wet season. Compounds with $KMD_{CH_2} \leq 0.11$ appear to be unsaturated carboxylic acids with the general molecular formulae $C_nH_{2n}O_2$, $C_nH_{2n}O_3$, $C_nH_{2n-2}O_2$ and $C_nH_{2n-2}O_4$. The elemental composition suggests fatty acids, which have been described in OA-related studies as essential compounds of marine and terrestrial vegetation (Stephanou and Stratigakis, 1993; Rincón et al., 2012; 770 Kourtchev et al., 2014b). Thus, long-range transport of marine aerosols or BBOA could explain the greater abundance of fatty acids during the dry season (Oros and Simoneit, 2001; Tervahattu et al., 2002). In addition, a large number of CHOS compounds with $KMD_{CH_2} \geq 0.21$ were detected exclusively during the dry season. Similar results were reported by Kourtchev et al. (2016), who found a larger number of homologous series of CHOS compounds in aerosol samples affected by anthropogenic emissions. These species are presumably highly oxygenated organosulfates, which are probably formed by 775 heterogeneous reactions on acidic sulfate particles.

Another interesting ion was detected at m/z 186.1135 ($C_9H_{17}NO_3$) with high signal intensities, especially during the dry season 2018. This compound has already been observed in biomass burning chamber experiments and field measurements in the Amazon rainforest (Laskin et al., 2009; Kourtchev et al., 2016). In the present study, Kendrick mass analysis revealed evidence of a homologous series, which is shown in the KMD plot in Figure 7. The general molecular formula can be described as $C_nH_{2n-1}NO_3$, where n ranges from 3 to 17 depending on the filter sample. The elemental composition initially suggested a nitrooxy functional group ($-ONO_2$), but MS² experiments (Figure S-184) did not show the typical nitrate fragment. Instead, the observed fragments indicated the presence of a carbamate functional group (R-NH-COOH). Due to their zwitterionic structure, these species could be relevant for condensed phase chemistry in the atmosphere, similar to amino acids (Mopper and Zika, 1987; Milne and Zika, 1993; McGregor and Anastasio, 2001; Barbaro et al., 2011). 780

785

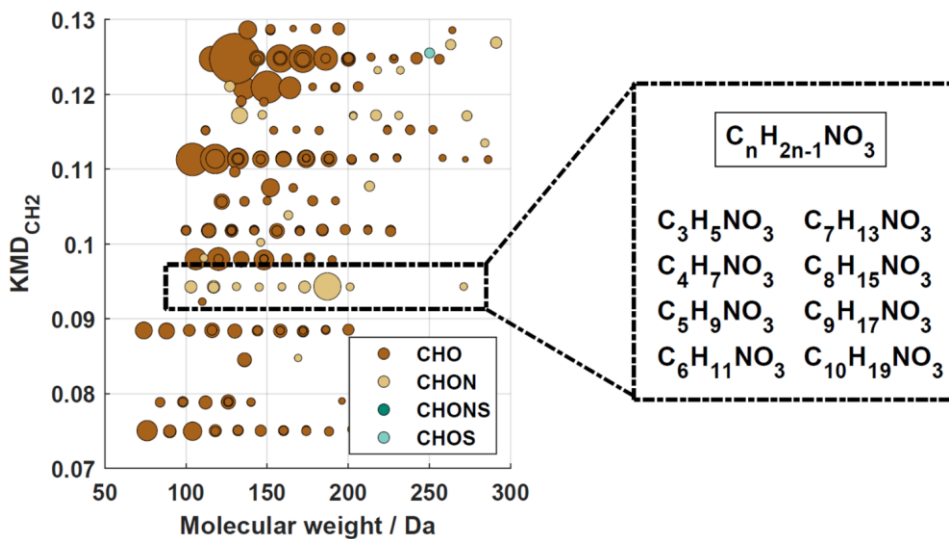


Figure 7: Kendrick mass defect diagram for the dry season 2018. The size of the data points represents the signal intensity of the corresponding peak. The four subgroups are distinguished with different colors. The dashed box highlights a homologous series of CHON compounds with a molecular formula of $C_n H_{2n-1} NO_3$ with $n = (3 - 17)$, potentially related to biomass burning emissions.

790 4 Conclusion

The organic chemical composition of atmospheric OA particles from the Amazon rainforest was investigated at the ATTO station using high-resolution MS in combination with an UHPLC system. Between 2018 and 2019, a total of four measurement campaigns were carried out, including two dry and wet seasons, with one "clean" wet period, one wet period influenced by biomass burning and combustion activities and two "polluted" dry periods. This allows conclusions to be drawn about seasonal influences in a unique ecosystem that is characterized by the complex interaction of numerous emission sources. In this analysis, a distinction was made between background compounds with a relatively low variability over time, and compounds with a much higher variability in their concentrations.

The results show a high fraction of isomeric structures in each data set, highlighting the need to use chromatographic separation methods for molecular identification of the aerosol components. Such an approach allows the reliable identification and quantification of a number of important marker compounds if reference compounds are available. However, the semi-quantitative determination of other compound classes is also possible, particularly by reducing ion suppression. The majority of compounds measured in both seasons had molecular weights (MW) below 250 Da. In addition, the analysis of the dry season samples showed signals in the oligomeric range between 300 and 450 Da with lower intensities. In general, the background molecular composition of organic aerosols at ATTO showed a clear seasonality with large differences between the dry and wet seasons. A considerable number of suitable marker compounds for different SOA sources were identified. The most important sources of background SOA at ATTO were the oxidation of isoprene and monoterpenes at both, high and low NOx concentrations and the formation of organosulfates. The results show that isoprene is the main precursor for S-containing SOA components at ATTO. The formation of isoprene OS probably occurs through the reactive uptake of IEPOX on acidic sulfate particles. It is assumed that in the wet season the sulfate particles reach the ATTO station mainly by long-range transport of marine aerosol, while in the dry season direct anthropogenic sources are also likely to be present. Furthermore, earlier studies showed that organic sulfur emissions from soils increase with higher soil water content which indicates a stronger

hat formatiert: Schriftfarbe: Text 1

organosulfur soil source from the forest itself in the wet seasons. Isoprene organosulfates can have both, purely biogenic and anthropogenic sources, whereby the biogenic sources appear to have a greater influence if the background OA composition is taken into account. This is further supported by the observation that the CHOS subgroup accounted for (8 ± 7) % in the wet season compared to only (3 ± 2) % in the dry season. Other dominant SOA groups that characterized the background were aromatic compounds whose source was most likely biomass burning. Thus, various oxygenated and nitrated hydrocarbons and oxidized polycyclic compounds showed significantly higher concentrations during the dry seasons. The evaluation of carbon oxidation states shows that LV-OOA and BBOA were the predominant and highly concentrated species in the dry seasons, while SV-OOA dominated in the wet seasons. We assume that a significant proportion of LV-OOA is formed by the aging and chemical processing of SOA components.

High signal intensities of nitroxyorganosulfates were observed in the dry seasons 2018 and 2019 as well as in the wet season 2019, whereby these were particularly derived from monoterpene precursors and correlated with the increased occurrence of fires and the SO_2 and NO_x concentrations. Noteworthy are the low vapor pressures of the CHONS compounds, which therefore make a significant contribution to ELVOCs. In addition, we find evidence of oligomeric structures of biogenic SOA components, as well as dimers of sesquiterpene oxidation products, which could also contribute to the ELVOC fraction. At the same time, a large fraction of BBOA contributes to the total OA, as shown by the high X_c values. Consequently, unsaturated and aromatic compounds such as nitrocatechols and nitrophenols were mainly attributed to deforestation fires, which occurred mainly during the dry periods. Interestingly, the chemical composition of OA particles from the 2019 wet season revealed a similar OA composition as in the dry season, suggesting that combustion emissions played a larger role in the wet season 2019. Fossil fuel combustion in Europe or strong biomass burning in the Sahel savanna regions could be responsible via long-distance transportation across the Atlantic. Follow up studies to address these different long-range transport scenarios in dedicated case studies, providing a more detailed understanding of their respective contributions are in preparation.

hat formatiert: Schriftfarbe: Text 1

835 **Data availability**

The data sets are available at upon registration at <https://www.attodata.org> (last access: 25 January 2022), and more information can be given by Thorsten Hoffmann (t.hoffmann@uni-mainz.de).

hat formatiert: Schriftfarbe: Text 1

Author contributions

840 DL and SH contributed equally. DL, SH and TH planned and designed the study. DL conducted the aerosol sampling, the sample preparation and analysis, the evaluation and wrote the manuscript. SH conducted the method validation of sample preparation and analysis, the evaluation and wrote the manuscript. NZ helped to collect the aerosol samples and revised the manuscript. LK, BH, JW, CP, and SW provided the SMPS and trace gas data. The meteorological data was provided by MS. MCS and UP provided scientific input and revised the manuscript. All authors contributed to the discussion of the results as well as the finalization of the manuscript.

Competing interests

The contact author has declared that none of the authors has any competing interests.

850 **Financial support**

This research has been supported by the German Federal Ministry of Education and Research (BMBF, grant no. 01LK1602D)); the Brazilian Ministério da Ciência, Tecnologia e Inovação (MCTI/FINEP); the Amazon State University (UEA); Fundação de Amparo à Pesquisa do Estado do Amazonas (FAPEAM); LBA/INPA; and SDS/CEUC/RDS-Uatumã and the German Research Foundation (Deutsche Forschungsgemeinschaft DFG: HO 1748/19-1; HO 1748/23-1; TRR 301 – Project-ID 428312742).

This open-access publication was funded by Johannes Gutenberg University Mainz.

860 **Acknowledgments**

For the operation of the ATTO site, we acknowledge the support by the German Federal Ministry of Education and Research (BMBF Contract 01LK1602D) and the Brazilian Ministério da Ciência, Tecnologia e Inovação (MCTI/FINEP) as well as the Amazon State University (UEA), FAPEAM, LBA/INPA, and SDS/CEUC/RDS-Uatumã. We also acknowledge the support of the Max Planck Society, and the Max Planck Graduate Center with the Johannes Gutenberg University Mainz (MPGC) and the Instituto Nacional de Pesquisas da Amazonia (INPA). Furthermore, we thank Florian Ditas and Maria Prass for help providing SMPS data. Particularly, we would like to thank the ATTO team members including Susan Trumbore, Alberto Quesada, Bruno Takeshi, Reiner Ditz, Stefan Wolff, Björn Nillius, Fernando Morais, Thomas Klimach, Roberta Pereira de Souza, Jürgen Kesselmeier, Andrew Crozier, Sam Jones, Delano Campos, Juarez Viegas, Sipko Bulthuis, Francisco Alcinei Gomes da Silva, Isabella Diogenes, Hermes Braga Xavier, Nagib Alberto de Castro Souza, Antonio Huxley Melo Nascimento, Valmir Ferreira de Lima, Feliciano de Souza Coelho, André Luiz Matos, Wallace Rabelo Costa, Amauri Rodrigues Perreira, Adir Vasconcelos Brandão, Davirley Gomes Silva, Thomas Disper, Torsten Helmer, Steffen Schmidt, Uwe Schulz, Uwe Schultz, Karl Kübler, Olaf Kolle, Martin Hertel, Kerstin Hippler, Steffen Schmidt and all further colleagues involved in the technical, logistical, and scientific support.

875

References

- 880 Andreae, M. O., Acevedo, O. C., Araújo, A., Artaxo, P., Barbosa, C. G. G., Barbosa, H. M. J., Brito, J., Carbone, S., Chi, X.,
Cintra, B. B. L., da Silva, N. F., Dias, N. L., Dias-Júnior, C. Q., Ditas, F., Ditz, R., Godoi, A. F. L., Godoi, R. H. M.,
Heimann, M., Hoffmann, T., Kesselmeier, J., Könemann, T., Krüger, M. L., Lavric, J. V., Manzi, A. O., Lopes, A.
P., Martins, D. L., Mikhailov, E. F., Moran-Zuloaga, D., Nelson, B. W., Nölscher, A. C., Santos Nogueira, D.,
Piedade, M. T. F., Pöhlker, C., Pöschl, U., Quesada, C. A., Rizzo, L. V., Ro, C.-U., Ruckteschler, N., Sá, L. D. A.,
Oliveira Sá, M. de, Sales, C. B., dos Santos, R. M. N., Saturno, J., Schöngart, J., Sörgel, M., Souza, C. M. de, Souza,
885 R. A. F. de, Su, H., Targhetta, N., Tóta, J., Trebs, I., Trumbore, S., van Eijck, A., Walter, D., Wang, Z., Weber, B.,
Williams, J., Winderlich, J., Wittmann, F., Wolff, S., and Yáñez-Serrano, A. M.: The Amazon Tall Tower
Observatory (ATTO): Overview of pilot measurements on ecosystem ecology, meteorology, trace gases, and aerosols,
Atmos. Chem. Phys., 15, 10723–10776, <https://doi.org/10.5194/acp-15-10723-2015>, 2015.
- Artaxo, P. et al.: Tropical and Boreal Forest – Atmosphere Interactions: A Review. *Tellus B: Chemical and Physical
Meteorology*, 74, 24–163, <https://doi.org/10.16993/tellusb.34>, 2022.
- 890 Artaxo, P., Rizzo, L. V., Brito, J. F., Barbosa, H. M. J., Arana, A., Sena, E. T., Cirino, G. G., Bastos, W., Martin, S. T., and
Andreae, M. O.: Atmospheric aerosols in Amazonia and land use change: From natural biogenic to biomass burning
conditions, *Faraday Discuss.*, 165, 203, <https://doi.org/10.1039/c3fd00052d>, 2013.
- Artaxo, P.: Physical and chemical properties of aerosols in the wet and dry seasons in Rondônia, Amazonia, *J. Geophys. Res.*,
107, 1052, <https://doi.org/10.1029/2001JD000666>, 2002.
- 895 Baccini, A., Goetz, S. J., Walker, W. S., Laporte, N. T., Sun, M., Sulla-Menashe, D., Hackler, J., Beck, P. S. A., Dubayah, R.,
Friedl, M. A., Samanta, S., and Houghton, R. A.: Estimated carbon dioxide emissions from tropical deforestation
improved by carbon-density maps, *Nature Clim. Change*, 2, 182–185, <https://doi.org/10.1038/nclimate1354>, 2012.
- Badertscher, M., Bischofberger, K., Munk, M. E., and Pretsch, E.: A novel formalism to characterize the degree of unsaturation
of organic molecules, *J. Chem. Inf. Comput. Sci.*, 41, 889–893, <https://doi.org/10.1021/ci000135o>, 2001.
- 900 Bateman, A. P., Walser, M. L., Desyaterik, Y., Laskin, J., Laskin, A., and Nizkorodov, S. A.: The effect of solvent on the
analysis of secondary organic aerosol using electrospray ionization mass spectrometry, *Environ. Sci. Technol.*, 42,
7341–7346, <https://doi.org/10.1021/es801226w>, 2008.
- Bates, K. H. and Jacob, D. J.: A new model mechanism for atmospheric oxidation of isoprene: global effects on oxidants,
nitrogen oxides, organic products, and secondary organic aerosol, *Atmos. Chem. Phys.*, 19, 9613–9640,
905 <https://doi.org/10.5194/acp-19-9613-2019>, 2019.
- Baumann, K., Wietzorek, M., Shahpoury, P., Filippi, A., Hildmann, S., Lelieveld, S., Berkemeier, T., Tong, H., Pöschl, U.
and Lammel, G.: Is the oxidative potential of components of fine particulate matter surface-mediated?, *Environ. Sci.
Pollut. Res.*, 30(6), 16749–16755. <https://doi.org/10.1007/s11356-022-24897-3>, 2023.
- Bianchi, F., Tröstl, J., Junninen, H., Frege, C., Henne, S., Hoyle, C. R., Molteni, U., Herrmann, E., Adamov, A., Bukowiecki,
910 N., Chen, X., Duplissy, J., Gysel, M., Hutterli, M., Kangasluoma, J., Kontkanen, J., Kürten, A., Manninen, H. E.,
Münch, S., Peräkylä, O., Petäjä, T., Rondo, L., Williamson, C., Weingartner, E., Curtius, J., Worsnop, D. R., Kulmala,
M., Dommen, J., and Baltensperger, U.: New particle formation in the free troposphere: A question of chemistry and
timing, *Science (New York, N.Y.)*, 352, 1109–1112, <https://doi.org/10.1126/science.aad5456>, 2016.
- Bruns, E. A., Krapf, M., Orasche, J., Huang, Y., Zimmermann, R., Drinovec, L., Močnik, G., El-Haddad, I., Slowik, J. G.,
915 Dommen, J., Baltensperger, U., and Prévôt, A. S. H.: Characterization of primary and secondary wood combustion
products generated under different burner loads, *Atmos. Chem. Phys.*, 15, 2825–2841, <https://doi.org/10.5194/acp-15-2825-2015>, 2015.

- Burgay, F., Salionov, D., Huber, C.J., Singer, T., Eichler, A., Ungeheuer, F., Vogel, A., Schwikowski, M., Bjelic, S., Hybrid Targeted/Untargeted Screening Method for the Determination of Wildfire and Water-Soluble Organic Tracers in Ice Cores and Snow, *Anal. Chem.*, 95(30), 11456-11466, <https://doi.org/10.1021/acs.analchem.3c01852>, 2023.
- 920 Chan, A. W. H., Kautzman, K. E., Chhabra, P. S., Surratt, J. D., Chan, M. N., Crounse, J. D., Kürten, A., Wennberg, P. O., Flagan, R. C., and Seinfeld, J. H.: Secondary organic aerosol formation from photooxidation of naphthalene and alkylnaphthalenes: implications for oxidation of intermediate volatility organic compounds (IVOCs), *Atmos. Chem. Phys.*, 9, 3049–3060, <https://doi.org/10.5194/acp-9-3049-2009>, 2009.
- 925 Chen, J. and Griffin, R.: Modeling secondary organic aerosol formation from oxidation of α -pinene, β -pinene, and γ -limonene, *Atmos. Environ.*, 39, 7731–7744, <https://doi.org/10.1016/j.atmosenv.2005.05.049>, 2005.
- Chen, Y., Takeuchi, M., Nah, T., Xu, L., Canagaratna, M. R., Stark, H., Baumann, K., Canonaco, F., Prévôt, A. S. H., Huey, L. G., Weber, R. J., and Ng, N. L.: Chemical characterization of secondary organic aerosol at a rural site in the southeastern US: insights from simultaneous high-resolution time-of-flight aerosol mass spectrometer (HR-ToF-AMS) and FIGAERO chemical ionization mass spectrometer (CIMS) measurements, *Atmos. Chem. Phys.*, 20, 8421–8440, <https://doi.org/10.5194/acp-20-8421-2020>, 2020.
- 930 Chhabra, P. S., Lambe, A. T., Canagaratna, M. R., Stark, H., Jayne, J. T., Onasch, T. B., Davidovits, P., Kimmel, J. R., and Worsnop, D. R.: Application of high-resolution time-of-flight chemical ionization mass spectrometry measurements to estimate volatility distributions of α -pinene and naphthalene oxidation products, *Atmos. Meas. Tech.*, 8, 1–18, <https://doi.org/10.5194/amt-8-1-2015>, 2015.
- 935 Claeys, M., Kourtchev, I., Pashynska, V., Vas, G., Vermeylen, R., Wang, W., Cafmeyer, J., Chi, X., Artaxo, P., Andreae, M. O., and Maenhaut, W.: Polar organic marker compounds in atmospheric aerosols during the LBA-SMOCC 2002 biomass burning experiment in Rondônia, Brazil: sources and source processes, time series, diel variations and size distributions, *Atmos. Chem. Phys.*, 10, 9319–9331, <https://doi.org/10.5194/acp-10-9319-2010>, 2010.
- 940 Claeys, M., Vermeylen, R., Yasmeen, F., Gómez-González, Y., Chi, X., Maenhaut, W., Mészáros, T., and Salma, I.: Chemical characterisation of humic-like substances from urban, rural and tropical biomass burning environments using liquid chromatography with UV/vis photodiode array detection and electrospray ionisation mass spectrometry, *Environ. Chem.*, 9, 273, <https://doi.org/10.1071/EN11163>, 2012.
- Claeys, M., Graham, B., Vas, G., Wang, W., Vermeylen, R., Pashynska, V., Cafmeyer, J., Guyon, P., Andreae, M. O., Artaxo, P., and Maenhaut, W.: Formation of secondary organic aerosols through photooxidation of isoprene, *Science (New York, N.Y.)*, 303, 1173–1176, <https://doi.org/10.1126/science.1092805>, 2004.
- 945 Clark, C. H., Nakao, S., Asa-Awuku, A., Sato, K., and Cocker, D. R.: Real-Time Study of Particle-Phase Products from α -Pinene Ozonolysis and Isoprene Photooxidation Using Particle into Liquid Sampling Directly Coupled to a Time-of-Flight Mass Spectrometer (PILS-ToF), *Aerosol Sci. Technol.*, 47, 1374–1382, <https://doi.org/10.1080/02786826.2013.844333>, 2013.
- 950 Daumit, K. E., Kessler, S. H., and Kroll, J. H.: Average chemical properties and potential formation pathways of highly oxidized organic aerosol, *Faraday Discuss.*, 165, 181–202, <https://doi.org/10.1039/c3fd00045a>, 2013.
- Donahue, N. M., Epstein, S. A., Pandis, S. N., and Robinson, A. L.: A two-dimensional volatility basis set: 1. organic-aerosol mixing thermodynamics, *Atmos. Chem. Phys.*, 11, 3303–3318, <https://doi.org/10.5194/acp-11-3303-2011>, 2011.
- 955 Eddingsaas, N. C., Loza, C. L., Yee, L. D., Chan, M., Schilling, K. A., Chhabra, P. S., Seinfeld, J. H., and Wennberg, P. O.: α -pinene photooxidation under controlled chemical conditions – Part 2: SOA yield and composition in low- and high-NO_x environments, *Atmos. Chem. Phys.*, 12, 7413–7427, <https://doi.org/10.5194/acp-12-7413-2012>, 2012.
- Florou, K., Blaziak, A., Jorga, S., Uruci, P., Vasilakopoulou, C.N., Szmigielski, R. and Pandis, S.N.: Properties and atmospheric oxidation of terebic acid aerosol, *ACS Earth Space Chem.*, 8(10), 2090-2100, <https://doi.org/10.1021/acsearthspacechem.4c00201>, 2024.
- 960

hat formatiert: Schriftfarbe: Text 1

- Frauenheim, M., Offenberg, J., Zhang, Z.F., Surratt, J.D., Gold, A.: Chemical composition of secondary organic aerosol formed from the oxidation of semivolatile isoprene epoxydiol isomerization products, *Environ. Sci. Technol.*, 58(51), 22571–22582, <https://doi.org/10.1021/acs.est.4c06850>, 2024.
- 965 Gao, L., Song, J., Mohr, C., Huang, W., Vallon, M., Jiang, F., Leisner, T., and Saathoff, H.: Kinetics, SOA yields, and chemical composition of secondary organic aerosol from β -caryophyllene ozonolysis with and without nitrogen oxides between 213 and 313 K, *Atmos. Chem. Phys.*, 22, 6001–6020, <https://doi.org/10.5194/acp-22-6001-2022>, 2022.
- Goldstein, A. H. and Galbally, I. E.: Known and unknown organic constituents in the Earth's atmosphere, *Environ. Sci. Technol.*, 41, 1514–1521, <https://doi.org/10.1021/es072476p>, 2007.
- 970 Gómez-González, Y., Wang, W., Vermeylen, R., Chi, X., Neiryneck, J., Janssens, I. A., Maenhaut, W., and Claeys, M.: Chemical characterisation of atmospheric aerosols during a 2007 summer field campaign at Brasschaat, Belgium: sources and source processes of biogenic secondary organic aerosol, *Atmos. Chem. Phys.*, 12, 125–138, <https://doi.org/10.5194/acp-12-125-2012>, 2012.
- Goulding, M. and Barthelm, R.: *The Smithsonian atlas of the Amazon*, Smithsonian Institution; Combined Academic, Washington, D.C., Chesham, 325 pp., 2003.
- 975 Greenberg, J. P., Guenther, A. B., Pétron, G., Wiedinmyer, C., Vega, O., Gatti, L. V., Tota, J., and Fisch, G.: Biogenic VOC emissions from forested Amazonian landscapes, *Global Change Biology*, 10, 651–662, <https://doi.org/10.1111/j.1365-2486.2004.00758.x>, 2004.
- Guenther, A., Hewitt, C. N., Erickson, D., Fall, R., Geron, C., Graedel, T., Harley, P., Klinger, L., Lerdau, M., McKay, W. A., Pierce, T., Scholes, B., Steinbrecher, R., Tallamraju, R., Taylor, J., and Zimmerman, P.: A global model of natural volatile organic compound emissions, *J. Geophys. Res.*, 100, 8873, <https://doi.org/10.1029/94JD02950>, 1995.
- 980 Guenther, A. B., Monson, R. K., and Fall, R.: Isoprene and monoterpene emission rate variability: Observations with eucalyptus and emission rate algorithm development, *J. Geophys. Res.*, 96, 10799, <https://doi.org/10.1029/91JD00960>, 1991.
- Hallquist, M., Wenger, J. C., Baltensperger, U., Rudich, Y., Simpson, D., Claeys, M., Dommen, J., Donahue, N. M., George, C., Goldstein, A. H., Hamilton, J. F., Herrmann, H., Hoffmann, T., Iinuma, Y., Jang, M., Jenkin, M. E., Jimenez, J. L., Kiendler-Scharr, A., Maenhaut, W., McFiggans, G., Mentel, T. F., Monod, A., Prévôt, A. S. H., Seinfeld, J. H., Surratt, J. D., Szmigielski, R., and Wildt, J.: The formation, properties and impact of secondary organic aerosol: current and emerging issues, *Atmos. Chem. Phys.*, 9, 5155–5236, <https://doi.org/10.5194/acp-9-5155-2009>, 2009.
- 985 Hammes, J., Lutz, A., Mentel, T., Faxon, C., and Hallquist, M.: Carboxylic acids from limonene oxidation by ozone and hydroxyl radicals: insights into mechanisms derived using a FIGAERO-CIMS, *Atmos. Chem. Phys.*, 19, 13037–13052, <https://doi.org/10.5194/acp-19-13037-2019>, 2019.
- Hennigan, C. J., Sullivan, A. P., Collett, J. L., and Robinson, A. L.: Levoglucosan stability in biomass burning particles exposed to hydroxyl radicals, *Geophys. Res. Lett.*, 37, n/a-n/a, <https://doi.org/10.1029/2010GL043088>, 2010.
- 990 Henze, D. K., Seinfeld, J. H., Ng, N. L., Kroll, J. H., Fu, T.-M., Jacob, D. J., and Heald, C. L.: Global modeling of secondary organic aerosol formation from aromatic hydrocarbons: high- vs. low-yield pathways, *Atmos. Chem. Phys.*, 8, 2405–2420, <https://doi.org/10.5194/acp-8-2405-2008>, 2008.
- Hettiyadura, A.P.S. and Laskin, A.: Quantitative analysis of polycyclic aromatic hydrocarbons using high-performance liquid chromatography-photodiode array-high-resolution mass spectrometric detection platform coupled to electrospray and atmospheric pressure photoionization sources, *J. Mass Spectrom.* 57(2), e4804, <https://doi.org/10.1002/jms.4804>, 2022.
- 1000 Hildmann, S., & Hoffmann, T.: Characterisation of atmospheric organic aerosols with one- and multidimensional liquid chromatography and mass spectrometry: State of the art and future perspectives. *TrAC Trends in Analytical Chemistry*, 175, 117698, <https://doi.org/10.1016/j.trac.2024.117698>, 2024.

hat formatiert: Englisch (Vereinigtes Königreich)

- Hoffmann, D., Tilgner, A., Iinuma, Y., and Herrmann, H.: Atmospheric stability of levoglucosan: a detailed laboratory and modeling study, *Environ. Sci. Technol.*, **44**, 694–699, <https://doi.org/10.1021/es902476f>, 2010.
- Hoffmann, T., Huang, R.-J., and Kalberer, M.: Atmospheric analytical chemistry, *Anal. Chem.*, **83**, 4649–4664, <https://doi.org/10.1021/ac2010718>, 2011.
- Holanda, B. A., Pöhlker, M. L., Walter, D., Saturno, J., Sörgel, M., Ditas, J., Ditas, F., Schulz, C., Franco, M. A., Wang, Q., Donth, T., Artaxo, P., Barbosa, H. M. J., Borrmann, S., Braga, R., Brito, J., Cheng, Y., Dollner, M., Kaiser, J. W., Klimach, T., Knote, C., Krüger, O. O., Fütterer, D., Lavrič, J. V., Ma, N., Machado, L. A. T., Ming, J., Morais, F. G., Paulsen, H., Sauer, D., Schlager, H., Schneider, J., Su, H., Weinzierl, B., Walser, A., Wendisch, M., Ziereis, H., Zöger, M., Pöschl, U., Andreae, M. O., and Pöhlker, C.: Influx of African biomass burning aerosol during the Amazonian dry season through layered transatlantic transport of black carbon-rich smoke, *Atmos. Chem. Phys.*, **20**, 4757–4785, <https://doi.org/10.5194/acp-20-4757-2020>, 2020.
- Holanda, B.A., Franco, M.A., Walter, D., Artaxo, P., Carbone, S., Cheng, Y., Chowdhury, S., Ditas, F., Gysel-Beer, M., Klimach, T., Krempel, L.A., Krüger, O.O., Lavric, J.V., Lelieveld, J., Ma, C., Machado, L.A.T., Modini, R.L., Morais, F.G., Pozzer, A., Saturno, J., Su, H., Wendisch, M., Wolff, S., Pöhlker, M.L., Andreae, M.O., Pöschl, U., & Pöhlker, C.: African biomass burning affects aerosol cycling over the Amazon, *Commun Earth Environ* **4**, 154, <https://doi.org/10.1038/s43247-023-00795-5>, 2023.
- Hughey, C. A., Hendrickson, C. L., Rodgers, R. P., Marshall, A. G., and Qian, K.: Kendrick Mass Defect Spectrum: A Compact Visual Analysis for Ultrahigh-Resolution Broadband Mass Spectra, *Anal. Chem.*, **73**, 4676–4681, <https://doi.org/10.1021/ac010560w>, 2001.
- Iinuma, Y., Böge, O., Gräfe, R., and Herrmann, H.: Methyl-nitrocatechols: atmospheric tracer compounds for biomass burning secondary organic aerosols, *Environmental science & technology*, **44**, 8453–8459, <https://doi.org/10.1021/es102938a>, 2010.
- INPE - Instituto Nacional de Pesquisas Espaciais, 2020: Portal do Monitoramento de Queimadas e Incêndios Florestais, Programa Queimadas, <http://www.inpe.br/queimadas>, last access: 14 December 2020.
- Jaoui, M., Szmigielski, R., Nestorowicz, K., Kolodziejczyk, A., Sarang, K., Rudzinski, K. J., Konopka, A., Bulska, E., Lewandowski, M., and Kleindienst, T. E.: Organic Hydroxy Acids as Highly Oxygenated Molecular (HOM) Tracers for Aged Isoprene Aerosol, *Environmental science & technology*, **53**, 14516–14527, <https://doi.org/10.1021/acs.est.9b05075>, 2019.
- Jenkin, M. E.: Modelling the formation and composition of secondary organic aerosol from α - and β - pinene ozonolysis using MCM v3, *Atmos. Chem. Phys.*, **4**, 1741–1757, <https://doi.org/10.5194/acp-4-1741-2004>, 2004.
- Jimenez, J. L., Canagaratna, M. R., Donahue, N. M., Prevot, A. S. H., Zhang, Q., Kroll, J. H., DeCarlo, P. F., Allan, J. D., Coe, H., Ng, N. L., Aiken, A. C., Docherty, K. S., Ulbrich, I. M., Grieshop, A. P., Robinson, A. L., Duplissy, J., Smith, J. D., Wilson, K. R., Lanz, V. A., Hueglin, C., Sun, Y. L., Tian, J., Laaksonen, A., Raatikainen, T., Rautiainen, J., Vaattovaara, P., Ehn, M., Kulmala, M., Tomlinson, J. M., Collins, D. R., Cubison, M. J., Dunlea, E. J., Huffman, J. A., Onasch, T. B., Alfarra, M. R., Williams, P. I., Bower, K., Kondo, Y., Schneider, J., Drewnick, F., Borrmann, S., Weimer, S., Demerjian, K., Salcedo, D., Cottrell, L., Griffin, R., Takami, A., Miyoshi, T., Hatakeyama, S., Shimono, A., Sun, J. Y., Zhang, Y. M., Dzepina, K., Kimmel, J. R., Sueper, D., Jayne, J. T., Herndon, S. C., Trimborn, A. M., Williams, L. R., Wood, E. C., Middlebrook, A. M., Kolb, C. E., Baltensperger, U., and Worsnop, D. R.: Evolution of organic aerosols in the atmosphere, *Science (New York, N.Y.)*, **326**, 1525–1529, <https://doi.org/10.1126/science.1180353>, 2009.
- Joo, T., Rivera-Rios, J. C., Takeuchi, M., Alvarado, M. J., and Ng, N. L.: Secondary Organic Aerosol Formation from Reaction of 3-Methylfuran with Nitrate Radicals, *ACS Earth Space Chem.*, **3**, 922–934, <https://doi.org/10.1021/acsearthspacechem.9b00068>, 2019.

hat formatiert: Schriftfarbe: Text 1

- Kahnt, A., Behrouzi, S., Vermeylen, R., Safi Shalamzari, M., Vercauteren, J., Roekens, E., Claeys, M., and Maenhaut, W.: One-year study of nitro-organic compounds and their relation to wood burning in PM10 aerosol from a rural site in Belgium, *Atmospheric Environment*, 81, 561–568, <https://doi.org/10.1016/j.atmosenv.2013.09.041>, 2013.
- 1050 Kanakidou, M., Seinfeld, J. H., Pandis, S. N., Barnes, I., Dentener, F. J., Facchini, M. C., van Dingenen, R., Ervens, B., Nenes, A., Nielsen, C. J., Swietlicki, E., Putaud, J. P., Balkanski, Y., Fuzzi, S., Horth, J., Moortgat, G. K., Winterhalter, R., Myhre, C. E. L., Tsigaridis, K., Vignati, E., Stephanou, E. G., and Wilson, J.: Organic aerosol and global climate modelling: a review, *Atmos. Chem. Phys.*, 5, 1053–1123, <https://doi.org/10.5194/acp-5-1053-2005>, 2005.
- Kautzman, K. E., Surratt, J. D., Chan, M. N., Chan, A. W. H., Hersey, S. P., Chhabra, P. S., Dalleska, N. F., Wennberg, P. O., Flagan, R. C., and Seinfeld, J. H.: Chemical composition of gas- and aerosol-phase products from the photooxidation of naphthalene, *The journal of physical chemistry. A*, 114, 913–934, <https://doi.org/10.1021/jp908530s>, 2010.
- 1055 Kendrick, E.: A Mass Scale Based on CH₂ = 14.0000 for High Resolution Mass Spectrometry of Organic Compounds, *Anal. Chem.*, 35, 2146–2154, <https://doi.org/10.1021/ac60206a048>, 1963.
- 1060 [Kesselmeier, J. and Staudt, M.: Biogenic Volatile Organic Compounds \(VOC\): An Overview on Emission, Physiology and Ecology, *Journal of Atmospheric Chemistry*, 33, 23–88, <https://doi.org/10.1023/A:1006127516791>, 1999.](#)
- Kitanovski, Z., Grđić, I., Yasmeen, F., Claeys, M., and Cusak, A.: Development of a liquid chromatographic method based on ultraviolet-visible and electrospray ionization mass spectrometric detection for the identification of nitrocatechols and related tracers in biomass burning atmospheric organic aerosol, *Rapid communications in mass spectrometry RCM*, 26, 793–804, <https://doi.org/10.1002/rcm.6170>, 2012.
- 1065 Kleindienst, T. E., Jaoui, M., Lewandowski, M., Offenberg, J. H., Lewis, C. W., Bhawe, P. V., and Edney, E. O.: Estimates of the contributions of biogenic and anthropogenic hydrocarbons to secondary organic aerosol at a southeastern US location, *Atmospheric Environment*, 41, 8288–8300, <https://doi.org/10.1016/j.atmosenv.2007.06.045>, 2007.
- Kong, X., Salvador, C. M., Carlsson, S., Pathak, R., Davidsson, K. O., Le Breton, M., Gaita, S. M., Mitra, K., Hallquist, Å. M., Hallquist, M., and Pettersson, J. B. C.: Molecular characterization and optical properties of primary emissions from a residential wood burning boiler, *The Science of the total environment*, 754, 142143, <https://doi.org/10.1016/j.scitotenv.2020.142143>, 2021.
- 1070 Kourtchev, I., Godoi, R.H.M., Connors, S., Levine, J.G., Archibald, A., Godoi, A.F.L., Paralovo, S., Barbosa, C.G.G., Souza, R.A.F., Manzi, A.O., Seco, R., Sjostedt, S., Park, J.-H., Guenther, A., Kim, S., Smith, J., Martin, S.T. and Kalberer, M.: Molecular composition of organic aerosols in central Amazonia: An ultra-high resolution mass spectrometry study, *Atmos. Chem. Phys.*, 16, 11899–11913, <https://doi.org/10.5194/acp-16-11899-2016>, 2016.
- 1075 Kourtchev, I., Fuller, S. J., Giorio, C., Healy, R. M., Wilson, E., O’Connor, I., Wenger, J. C., McLeod, M., Aalto, J., Ruuskanen, T. M., Maenhaut, W., Jones, R., Venables, D. S., Sodeau, J. R., Kulmala, M., and Kalberer, M.: Molecular composition of biogenic secondary organic aerosols using ultrahigh-resolution mass spectrometry: Comparing laboratory and field studies, *Atmos. Chem. Phys.*, 14, 2155–2167, <https://doi.org/10.5194/acp-14-2155-2014>, 2014a.
- 1080 Kourtchev, I., O’Connor, I. P., Giorio, C., Fuller, S. J., Kristensen, K., Maenhaut, W., Wenger, J. C., Sodeau, J. R., Glasius, M., and Kalberer, M.: Effects of anthropogenic emissions on the molecular composition of urban organic aerosols: An ultrahigh resolution mass spectrometry study, *Atmospheric Environment*, 89, 525–532, <https://doi.org/10.1016/j.atmosenv.2014.02.051>, 2014b.
- 1085 Kourtchev, I., Fuller, S., Aalto, J., Ruuskanen, T. M., McLeod, M. W., Maenhaut, W., Jones, R., Kulmala, M., and Kalberer, M.: Molecular composition of boreal forest aerosol from Hyytiälä, Finland, using ultrahigh resolution mass spectrometry, *Environmental science & technology*, 47, 4069–4079, <https://doi.org/10.1021/es3051636>, 2013.

hat formatiert: Englisch (Vereinigtes Königreich)

- 1090 Kourtchev, I., Sebben, B.G., Brill, S., Cybelli, G.G.B., Weber, B., Ferreira, R.R., D'Oliveira, F.A.F., Dias, C.Q. Jr., Popoola, O.A.M., Williams, J., Pöhlker, C., Godoi, R.H.M., Occurrence of a " forever chemical " in the atmosphere above pristine Amazon Forest, *Sci. Total Environ.*, 944, AR 173918, 10.1016/j.scitotenv.2024.173918, 2024.
- 1095 Krechmer, J. E., Coggon, M. M., Massoli, P., Nguyen, T. B., Crounse, J. D., Hu, W., Day, D. A., Tyndall, G. S., Henze, D. K., Rivera-Rios, J. C., Nowak, J. B., Kimmel, J. R., Mauldin, R. L., Stark, H., Jayne, J. T., Sipilä, M., Junninen, H., Clair, J. M. S., Zhang, X., Feiner, P. A., Zhang, L., Miller, D. O., Brune, W. H., Keutsch, F. N., Wennberg, P. O., Seinfeld, J. H., Worsnop, D. R., Jimenez, J. L., and Canagaratna, M. R.: Formation of Low Volatility Organic Compounds and Secondary Organic Aerosol from Isoprene Hydroxyhydroperoxide Low-NO Oxidation, *Environmental science & technology*, 49, 10330–10339, <https://doi.org/10.1021/acs.est.5b02031>, 2015.
- Kristensen, K., Enggrob, K. L., King, S. M., Worton, D. R., Platt, S. M., Mortensen, R., Rosenoern, T., Surratt, J. D., Bilde, M., Goldstein, A. H., and Glasius, M.: Formation and occurrence of dimer esters of pinene oxidation products in atmospheric aerosols, *Atmos. Chem. Phys.*, 13, 3763–3776, <https://doi.org/10.5194/acp-13-3763-2013>, 2013.
- 1100 Kroll, J. H. and Seinfeld, J. H.: Chemistry of secondary organic aerosol: Formation and evolution of low-volatility organics in the atmosphere, *Atmospheric Environment*, 42, 3593–3624, <https://doi.org/10.1016/j.atmosenv.2008.01.003>, 2008.
- Kroll, J. H., Donahue, N. M., Jimenez, J. L., Kessler, S. H., Canagaratna, M. R., Wilson, K. R., Altieri, K. E., Mazzoleni, L. R., Wozniak, A. S., Bluhm, H., Mysak, E. R., Smith, J. D., Kolb, C. E., and Worsnop, D. R.: Carbon oxidation state as a metric for describing the chemistry of atmospheric organic aerosol, *Nature chemistry*, 3, 133–139, <https://doi.org/10.1038/nchem.948>, 2011.
- 1105 Kundu, S., Fisseha, R., Putman, A. L., Rahn, T. A., and Mazzoleni, L. R.: High molecular weight SOA formation during limonene ozonolysis: insights from ultrahigh-resolution FT-ICR mass spectrometry characterization, *Atmos. Chem. Phys.*, 12, 5523–5536, <https://doi.org/10.5194/acp-12-5523-2012>, 2012.
- Laskin, A., Smith, J. S., and Laskin, J.: Molecular characterization of nitrogen-containing organic compounds in biomass burning aerosols using high-resolution mass spectrometry, *Environ. Sci. Technol.*, 43, 3764–3771, <https://doi.org/10.1021/es803456n>, 2009.
- 1110 Li, Y., Pöschl, U., and Shiraiwa, M.: Molecular corridors and parameterizations of volatility in the chemical evolution of organic aerosols, *Atmos. Chem. Phys.*, 16, 3327–3344, <https://doi.org/10.5194/acp-16-3327-2016>, 2016.
- 1115 Lin, P., Aiona, P. K., Li, Y., Shiraiwa, M., Laskin, J., Nizkorodov, S. A., and Laskin, A.: Molecular Characterization of Brown Carbon in Biomass Burning Aerosol Particles, *Environmental science & technology*, 50, 11815–11824, <https://doi.org/10.1021/acs.est.6b03024>, 2016.
- Lin, P., Rincon, A. G., Kalberer, M., and Yu, J. Z.: Elemental composition of HULIS in the Pearl River Delta Region, China: results inferred from positive and negative electrospray high resolution mass spectrometric data, *Environmental science & technology*, 46, 7454–7462, <https://doi.org/10.1021/es300285d>, 2012.
- 1120 Lin, P., Fleming, L.T., Nizkorodov, S.A., Laskin, J., Laskin, A.: Comprehensive Molecular Characterization of Atmospheric Brown Carbon by High Resolution Mass Spectrometry with Electrospray and Atmospheric, Pressure Photoionization, *Anal. Chem.*, 90(21), 12493–12502, <https://doi.org/10.1021/acs.analchem.8b02177>, 2018.
- 1125 Mazzoleni, L. R., Saranjampour, P., Dalbec, M. M., Samburova, V., Hallar, A. G., Zielinska, B., Lowenthal, D. H., and Kohl, S.: Identification of water-soluble organic carbon in non-urban aerosols using ultrahigh-resolution FT-ICR mass spectrometry: organic anions, *Environ. Chem.*, 9, 285, <https://doi.org/10.1071/EN11167>, 2012.
- [Mendonca, A.C.S., Dias-Junior, C.Q., Acevedo, O.C., Marra, D.M., Cely-Toro, I.M., Fisch, G., Brondani, D.V., Manzi, A.O., Portela, B.T.T., Quesada, C.A., Mortarini, L.: Estimation of the nocturnal boundary layer height over the Central Amazon forest using turbulence measurements, *Agriculture and Forest Meteorology*, 367, 110469, <https://doi.org/10.1016/j.agrformet.2025.110469>, 2025.](https://doi.org/10.1016/j.agrformet.2025.110469)

hat formatiert: Schriftfarbe: Text 1

hat formatiert: Nicht unterstrichen, Schriftfarbe: Text 1

- Mettler, M. S., Mushrif, S. H., Paulsen, A. D., Javadekar, A. D., Vlachos, D. G., and Dauenhauer, P. J.: Revealing pyrolysis chemistry for biofuels production: Conversion of cellulose to furans and small oxygenates, *Energy Environ. Sci.*, 5, 5414–5424, <https://doi.org/10.1039/C1EE02743C>, 2012.
- 1135 Molteni, U., Bianchi, F., Klein, F., El Haddad, I., Frege, C., Rossi, M. J., Dommen, J., and Baltensperger, U.: Formation of highly oxygenated organic molecules from aromatic compounds, 2016.
- Monks, P. S.: Gas-phase radical chemistry in the troposphere, *Chemical Society reviews*, 34, 376–395, <https://doi.org/10.1039/b307982c>, 2005.
- Murphy, B. N., Donahue, N. M., Robinson, A. L., and Pandis, S. N.: A naming convention for atmospheric organic aerosol, *Atmos. Chem. Phys.*, 14, 5825–5839, <https://doi.org/10.5194/acp-14-5825-2014>, 2014.
- 1140 Nagori, J., Janssen, R. H. H., Fry, J. L., Krol, M., Jimenez, J. L., Hu, W., and Vilà-Guerau de Arellano, J.: Biogenic emissions and land–atmosphere interactions as drivers of the daytime evolution of secondary organic aerosol in the southeastern US, *Atmos. Chem. Phys.*, 19, 701–729, <https://doi.org/10.5194/acp-19-701-2019>, 2019.
- Nguyen, T. B., Roach, P. J., Laskin, J., Laskin, A., and Nizkorodov, S. A.: Effect of humidity on the composition of isoprene photooxidation secondary organic aerosol, *Atmos. Chem. Phys.*, 11, 6931–6944, <https://doi.org/10.5194/acp-11-6931-2011>, 2011.
- 1145 Nguyen, T. B., Bateman, A. P., Bones, D. L., Nizkorodov, S. A., Laskin, J., and Laskin, A.: High- resolution mass spectrometry analysis of secondary organic aerosol generated by ozonolysis of isoprene, *Atmospheric Environment*, 44, 1032–1042, <https://doi.org/10.1016/j.atmosenv.2009.12.019>, 2010.
- Nizkorodov, S. A., Laskin, J., and Laskin, A.: Molecular chemistry of organic aerosols through the application of high resolution mass spectrometry, *Physical chemistry chemical physics PCCP*, 13, 3612–3629, <https://doi.org/10.1039/C0CP02032J>, 2011.
- 1150 Nolte, C. G., Schauer, J. J., Cass, G. R., and Simoneit, B. R.: Highly polar organic compounds present in wood smoke and in the ambient atmosphere, *Environ. Sci. Technol.*, 35, 1912–1919, <https://doi.org/10.1021/es001420r>, 2001.
- Nozière, B., Kalberer, M., Claeys, M., Allan, J., D'Anna, B., Decesari, S., Finessi, E., Glasius, M., Grgić, I., Hamilton, J. F., Hoffmann, T., Iinuma, Y., Jaoui, M., Kahnt, A., Kampf, C. J., Kourtev, I., Maenhaut, W., Marsden, N., Saarikoski, S., Schnelle-Kreis, J., Surratt, J. D., Szidat, S., Szmigielski, R., and Wisthaler, A.: The molecular identification of organic compounds in the atmosphere: state of the art and challenges, *Chemical reviews*, 115, 3919–3983, <https://doi.org/10.1021/cr5003485>, 2015.
- 1155 Odum, J. R., Hoffmann, T., Bowman, F., Collins, D. R., Flagan, R. C., and Seinfeld, J. H.: Gas/Particle Partitioning and Secondary Organic Aerosol Yields, *Environ. Sci. Technol.*, 30, 2580–2585, <https://doi.org/10.1021/es950943+>, 1996.
- Oros, D. R. and Simoneit, B. R.T.: Identification and emission factors of molecular tracers in organic aerosols from biomass burning Part 1. Temperate climate conifers, *Applied Geochemistry*, 16, 1513–1544, [https://doi.org/10.1016/S0883-2927\(01\)00021-X](https://doi.org/10.1016/S0883-2927(01)00021-X), 2001.
- 1160 Pankow, J. F.: An absorption model of the gas/aerosol partitioning involved in the formation of secondary organic aerosol, *Atmospheric Environment*, 28, 189–193, [https://doi.org/10.1016/1352-2310\(94\)90094-9](https://doi.org/10.1016/1352-2310(94)90094-9), 1994.
- Paulot, F., Crounse, J. D., Kjaergaard, H. G., Kurten, A., St Clair, J. M., Seinfeld, J. H., and Wennberg, P. O.: Unexpected epoxide formation in the gas-phase photooxidation of isoprene, *Science (New York, N.Y.)*, 325, 730–733, <https://doi.org/10.1126/science.1172910>, 2009.
- 1170 Peeters, J., Vereecken, L., and Fantechi, G.: The detailed mechanism of the OH-initiated atmospheric oxidation of α -pinene: a theoretical, *Physical chemistry chemical physics PCCP*, 3, 5489–5504, <https://doi.org/10.1039/b106555f>, 2001.
- [Pfannerstill, E. Y., Rejirink, N. G., Edtbauer, A., Ringsdorf, A., Zannoni, N., Araújo, A., Ditas, F., Holanda, B. A., Sá, M. O., Tsokankunku, A., Walter, D., Wolff, S., Lavrič, J. V., Pöhlker, C., Sörgel, M., and Williams, J.: Total OH reactivity](#)

over the Amazon rainforest: variability with temperature, wind, rain, altitude, time of day, season, and an overall budget closure. *Atmos. Chem. Phys.*, 21, 6231–6256, <https://doi.org/10.5194/acp-21-6231-2021>, 2021.

hat formatiert: Nicht unterstrichen, Schriftfarbe: Text 1

Pöhlker, M.L., Pöhlker, C., Quaas, J. et al. Global organic and inorganic aerosol hygroscopicity and its effect on radiative forcing. *Nat Commun* 14, 6139, <https://doi.org/10.1038/s41467-023-41695-8>, 2023.

hat formatiert: Schriftfarbe: Text 1

Pöhlker, M. L., Ditas, F., Saturno, J., Klimach, T., Hrabě de Angelis, I., Araújo, A. C., Brito, J., Carbone, S., Cheng, Y., Chi, X., Ditz, R., Gunthe, S. S., Holanda, B. A., Kandler, K., Kesselmeier, J., Könemann, T., Krüger, O. O., Lavrič, J. V., Martin, S. T., Mikhailov, E., Moran-Zuloaga, D., Rizzo, L. V., Rose, D., Su, H., Thalman, R., Walter, D., Wang, J., Wolff, S., Barbosa, H. M. J., Artaxo, P., Andreae, M. O., Pöschl, U., and Pöhlker, C.: Long-term observations of cloud condensation nuclei over the Amazon rain forest – Part 2: Variability and characteristics of biomass burning, long-range transport, and pristine rain forest aerosols, *Atmos. Chem. Phys.*, 18, 10289–10331, <https://doi.org/10.5194/acp-18-10289-2018>, 2018.

Pöhlker, C., Walter, D., Paulsen, H., Könemann, T., Rodríguez-Caballero, E., Moran-Zuloaga, D., Brito, J., Carbone, S., Degrendele, C., Després, V. R., Ditas, F., Holanda, B. A., Kaiser, J. W., Lammel, G., Lavrič, J. V., Ming, J., Pickersgill, D., Pöhlker, M. L., Praß, M., Löbs, N., Saturno, J., Sörgel, M., Wang, Q., Weber, B., Wolff, S., Artaxo, P., Pöschl, U., and Andreae, M. O.: Land cover and its transformation in the backward trajectory footprint region of the Amazon Tall Tower Observatory, *Atmos. Chem. Phys.*, 19, 8425–8470, <https://doi.org/10.5194/acp-19-8425-2019>, 2019.

Pöschl, U., Martin, S. T., Sinha, B., Chen, Q., Gunthe, S. S., Huffman, J. A., Borrmann, S., Farmer, D. K., Garland, R. M., Helas, G., Jimenez, J. L., King, S. M., Manzi, A., Mikhailov, E., Pauliquevis, T., Petters, M. D., Prenni, A. J., Roldin, P., Rose, D., Schneider, J., Su, H., Zorn, S. R., Artaxo, P., and Andreae, M. O.: Rainforest aerosols as biogenic nuclei of clouds and precipitation in the Amazon, *Science (New York, N.Y.)*, 329, 1513–1516, <https://doi.org/10.1126/science.1191056>, 2010.

Pöschl, U.: Atmospheric aerosols: composition, transformation, climate and health effects, *Angewandte Chemie (International ed. in English)*, 44, 7520–7540, <https://doi.org/10.1002/anie.200501122>, 2005.

Pugliese, G., Ingrisch, J., Meredith, L.K. et al. Effects of drought and recovery on soil volatile organic compound fluxes in an experimental rainforest. *Nat Commun* 14, 5064, <https://doi.org/10.1038/s41467-023-40661-8>, 2023.

hat formatiert: Schriftfarbe: Text 1

Putman, A. L., Offenberg, J. H., Fisseha, R., Kundu, S., Rahn, T. A., and Mazzoleni, L. R.: Ultrahigh-resolution FT-ICR mass spectrometry characterization of α -pinene ozonolysis SOA, *Atmospheric Environment*, 46, 164–172, <https://doi.org/10.1016/j.atmosenv.2011.10.003>, 2012.

Reinhardt, A., Emmenegger, C., Gerrits, B., Panse, C., Dommen, J., Baltensperger, U., Zenobi, R., and Kalberer, M.: Ultrahigh mass resolution and accurate mass measurements as a tool to characterize oligomers in secondary organic aerosols, *Anal. Chem.*, 79, 4074–4082, <https://doi.org/10.1021/ac062425v>, 2007.

Rincón, A. G., Calvo, A. I., Dietzel, M., and Kalberer, M.: Seasonal differences of urban organic aerosol composition – an ultra-high resolution mass spectrometry study, *Environ. Chem.*, 9, 298, <https://doi.org/10.1071/EN12016>, 2012.

Rolph, G., Stein, A., and Stunder, B.: Real-time Environmental Applications and Display sYstem: READY, *Environmental Modelling & Software*, 95, 210–228, <https://doi.org/10.1016/j.envsoft.2017.06.025>, 2017.

Samburova, V., Connolly, J., Gyawali, M., Yatavelli, R. L. N., Watts, A. C., Chakrabarty, R. K., Zielinska, B., Moosmüller, H., and Khlystov, A.: Polycyclic aromatic hydrocarbons in biomass-burning emissions and their contribution to light absorption and aerosol toxicity, *The Science of the total environment*, 568, 391–401, <https://doi.org/10.1016/j.scitotenv.2016.06.026>, 2016.

- Schauer, J. J., Kleeman, M. J., Cass, G. R., and Simoneit, B. R.: Measurement of emissions from air pollution sources. 3. C1-C29 organic compounds from fireplace combustion of wood, *Environ. Sci. Technol.*, 35, 1716–1728, <https://doi.org/10.1021/es001331e>, 2001.
- Seinfeld, J. H. and Pandis, S. N.: *Atmospheric Chemistry and Physics: From Air Pollution to Climate Change*, 3rd ed., John Wiley & Sons, 944 s, 2016.
- Seinfeld, J. H. and Pankow, J. F.: Organic atmospheric particulate material, *Annual review of physical chemistry*, 54, 121–140, <https://doi.org/10.1146/annurev.physchem.54.011002.103756>, 2003.
- Shiraiwa, M., Berkemeier, T., Schilling-Fahnestock, K. A., Seinfeld, J. H., and Pöschl, U.: Molecular corridors and kinetic regimes in the multiphase chemical evolution of secondary organic aerosol, *Atmos. Chem. Phys.*, 14, 8323–8341, <https://doi.org/10.5194/acp-14-8323-2014>, 2014.
- Shrivastava, M., Andreae, M.O., Artaxo, P., Barbosa, H.M., Berg, L.K., Brito, J., Ching, J., Easter, R.C., Fan, J., Fast, J.D. and Feng, Z.: Urban pollution greatly enhances formation of natural aerosols over the Amazon rainforest, *Nature Communications*, 10, <https://doi.org/10.1038/s41467-019-08909-4>, 2019.
- Siemens, K.S.A., Pagonis, D., Guo, H.Y., Schueneman, M.K., Dibb, J.E., Campuzano-Jost, P., Jimenez, J.L. and Laskin, A.: Probing Atmospheric Aerosols by Multimodal Mass Spectrometry Techniques: Revealing Aging Characteristics of Its Individual Molecular Components, *ACS Earth Space Chem.* 7(12), 2498-2510, <https://doi.org/10.1021/acsearthspacechem.3c00228>, 2023.
- Simoneit, B.R.T., Schauer, J. J., Nolte, C. G., Oros, D. R., Elias, V. O., Fraser, M. P., Rogge, W. F., and Cass, G. R.: Levoglucosan, a tracer for cellulose in biomass burning and atmospheric particles, *Atmospheric Environment*, 33, 173–182, [https://doi.org/10.1016/S1352-2310\(98\)00145-9](https://doi.org/10.1016/S1352-2310(98)00145-9), 1999.
- Stein, A. F., Draxler, R. R., Rolph, G. D., Stunder, B. J. B., Cohen, M. D., and Ngan, F.: NOAA’s HYSPLIT Atmospheric Transport and Dispersion Modeling System, *Bulletin of the American Meteorological Society*, 96, 2059–2077, <https://doi.org/10.1175/BAMS-D-14-00110.1>, 2015.
- Stephanou, E. G. and Stratigakos, N.: Oxocarboxylic and α,ω -dicarboxylic acids: photooxidation products of biogenic unsaturated fatty acids present in urban aerosols, *Environ. Sci. Technol.*, 27, 1403–1407, <https://doi.org/10.1021/es00044a016>, 1993.
- Surratt, J. D., Gómez-González, Y., Chan, A. W. H., Vermeylen, R., Shahgholi, M., Kleindienst, T. E., Edney, E. O., Offenberg, J. H., Lewandowski, M., Jaoui, M., Maenhaut, W., Claeys, M., Flagan, R. C., and Seinfeld, J. H.: Organosulfate formation in biogenic secondary organic aerosol, *The journal of physical chemistry. A*, 112, 8345–8378, <https://doi.org/10.1021/jp802310p>, 2008.
- Surratt, J. D., Kroll, J. H., Kleindienst, T. E., Edney, E. O., Claeys, M., Sorooshian, A., Ng, N. L., Offenberg, J. H., Lewandowski, M., Jaoui, M., Flagan, R. C., and Seinfeld, J. H.: Evidence for Organosulfates in Secondary Organic Aerosol, *Environ. Sci. Technol.*, 41, 517–527, <https://doi.org/10.1021/es062081q>, 2007.
- Szmigielski, R., Surratt, J. D., Gómez-González, Y., van der Veken, P., Kourtchev, I., Vermeylen, R., Blockhuys, F., Jaoui, M., Kleindienst, T. E., Lewandowski, M., Offenberg, J. H., Edney, E. O., Seinfeld, J. H., Maenhaut, W., and Claeys, M.: 3-methyl-1,2,3-butanetricarboxylic acid: An atmospheric tracer for terpene secondary organic aerosol, *Geophys. Res. Lett.*, 34, D16312, <https://doi.org/10.1029/2007GL031338>, 2007.
- Tervahattu, H., Juhanaja, J., and Kupiainen, K.: Identification of an organic coating on marine aerosol particles by TOF-SIMS, *J. Geophys. Res.*, 107, <https://doi.org/10.1029/2001JD001403>, 2002.
- Thoma, M., Bachmeier, F., Gottwald, F.L., Simon, M., Vogel, A.L.: Mass spectrometry-based Aerosolomics: A new approach to resolve sources, composition, and partitioning of secondary organic aerosol, *Atmos. Meas. Techn.* 15(23), 7137–7154, <https://doi.org/10.5194/amt-15-7137-2022>, 2022.

hat formatiert: Schriftfarbe: Text 1

- Tolocka, M. P., Jang, M., Ginter, J. M., Cox, F. J., Kamens, R. M., and Johnston, M. V.: Formation of Oligomers in Secondary Organic Aerosol, *Environ. Sci. Technol.*, 38, 1428–1434, <https://doi.org/10.1021/es035030r>, 2004.
- 1260 Tong, H., Kourtchev, I., Pant, P., Keyte, I. J., O'Connor, I. P., Wenger, J. C., Pope, F. D., Harrison, R. M., and Kalberer, M.: Molecular composition of organic aerosols at urban background and road tunnel sites using ultra-high resolution mass spectrometry, *Faraday Discuss.*, 189, 51–68, <https://doi.org/10.1039/c5fd00206k>, 2016.
- Tu, P., Hall, W. A., and Johnston, M. V.: Characterization of Highly Oxidized Molecules in Fresh and Aged Biogenic Secondary Organic Aerosol, *Analytical chemistry*, 88, 4495–4501, <https://doi.org/10.1021/acs.analchem.6b00378>, 2016.
- 1265 Wang, X., Hayeck, N., Brüggemann, M., Yao, L., Chen, H., Zhang, C., Emmelin, C., Chen, J., George, C., and Wang, L.: Chemical Characteristics of Organic Aerosols in Shanghai: A Study by Ultrahigh-Performance Liquid Chromatography Coupled With Orbitrap Mass Spectrometry, *J. Geophys. Res.*, 122, 11,703–11,722, <https://doi.org/10.1002/2017JD026930>, 2017.
- 1270 Worton, D. R., Surratt, J. D., Lafranchi, B. W., Chan, A. W. H., Zhao, Y., Weber, R. J., Park, J.-H., Gilman, J. B., Gouw, J. de, Park, C., Schade, G., Beaver, M., Clair, J. M. S., Crounse, J., Wennberg, P., Wolfe, G. M., Harrold, S., Thornton, J. A., Farmer, D. K., Docherty, K. S., Cubison, M. J., Jimenez, J.-L., Frossard, A. A., Russell, L. M., Kristensen, K., Glasius, M., Mao, J., Ren, X., Brune, W., Browne, E. C., Pusede, S. E., Cohen, R. C., Seinfeld, J. H., and Goldstein, A. H.: Observational insights into aerosol formation from isoprene, *Environmental science & technology*, 47, 11403–11413, <https://doi.org/10.1021/es4011064>, 2013.
- 1275 Wozniak, A. S., Bauer, J. E., Sleighter, R. L., Dickhut, R. M., and Hatcher, P. G.: Technical Note: Molecular characterization of aerosol-derived water soluble organic carbon using ultrahigh resolution electrospray ionization Fourier transform ion cyclotron resonance mass spectrometry, *Atmos. Chem. Phys.*, 8, 5099–5111, <https://doi.org/10.5194/acp-8-5099-2008>, 2008.
- Xie, Q.R. and Laskin, A.: Molecular characterization of atmospheric organic aerosols: Contemporary applications of high-resolution mass spectrometry, *TrAC, Trends Anal. Chem.* 181. <https://doi.org/10.1016/j.trac.2024.117986>, 2024.
- 1280 Yáñez-Serrano, A. M., Nölscher, A. C., Boutsoukidis, E., Gomes Alves, E., Ganzeveld, L., Bonn, B., Wolff, S., Sa, M., Yamasoe, M., Williams, J., Andreae, M. O., and Kesselmeier, J.: Monoterpene chemical speciation in a tropical rainforest: variation with season, height, and time of day at the Amazon Tall Tower Observatory (ATTO), *Atmos. Chem. Phys.*, 18, 3403–3418, <https://doi.org/10.5194/acp-18-3403-2018>, 2018.
- 1285 Yassine, M. M., Harir, M., Dabek-Zlotorzynska, E., and Schmitt-Kopplin, P.: Structural characterization of organic aerosol using Fourier transform ion cyclotron resonance mass spectrometry: aromaticity equivalent approach, *Rapid communications in mass spectrometry RCM*, 28, 2445–2454, <https://doi.org/10.1002/rcm.7038>, 2014.
- Zannoni, N., Leppla, D., Lembo Silveira de Assis, P.I. et al. Surprising chiral composition changes over the Amazon rainforest with height, time and season. *Commun Earth Environ* 1, 4. <https://doi.org/10.1038/s43247-020-0007-9>, 2020.
- 1290 Zhang, Q., Jimenez, J. L., Canagaratna, M. R., Allan, J. D., Coe, H., Ulbrich, I., Alfarra, M. R., Takami, A., Middlebrook, A. M., Sun, Y. L., Dzepina, K., Dunlea, E., Docherty, K., DeCarlo, P. F., Salcedo, D., Onasch, T., Jayne, J. T., Miyoshi, T., Shimojo, A., Hatakeyama, S., Takegawa, N., Kondo, Y., Schneider, J., Drewnick, F., Borrmann, S., Weimer, S., Demerjian, K., Williams, P., Bower, K., Bahreini, R., Cottrell, L., Griffin, R. J., Rautiainen, J., Sun, J. Y., Zhang, Y. M., and Worsnop, D. R.: Ubiquity and dominance of oxygenated species in organic aerosols in anthropogenically-influenced Northern Hemisphere midlatitudes, *Geophys. Res. Lett.*, 34, n/a-n/a, <https://doi.org/10.1029/2007GL029979>, 2007.
- 1295 Zhang, W., Wang, W., Li, J., Peng, C., Li, K., Zhou, L., Shi, B., Chen, Y., Liu, M., Ge, M.: Effects of SO₂ on optical properties of secondary organic aerosol generated from photooxidation of toluene under different relative humidity conditions. *Atmos. Chem. Phys.*, 20, 4477–4492. <https://doi.org/10.5194/acp-20-4477-2020>.

hat formatiert: Schriftfarbe: Text 1

hat formatiert: Englisch (Vereinigtes Königreich)

hat formatiert: Nicht unterstrichen, Schriftfarbe: Text 1

hat formatiert: Englisch (Vereinigtes Königreich)

- 1300 Zhang, Y. Y., Müller, L., Winterhalter, R., Moortgat, G. K., Hoffmann, T., and Pöschl, U.: Seasonal cycle and temperature dependence of pinene oxidation products, dicarboxylic acids and nitrophenols in fine and coarse air particulate matter, *Atmos. Chem. Phys.*, 10, 7859–7873, <https://doi.org/10.5194/acp-10-7859-2010>, 2010.
- Zhang Y, Wang K, Tong H, Huang RJ, Hoffmann T.: The maximum carbonyl ratio (MCR) as a new index for the structural classification of secondary organic aerosol components. *Rapid Commun Mass Spectrom*, 35(14):e9113. doi: 10.1002/rcm.9113, 2021.